
ADAPTIVE ACCOUNTABILITY IN NETWORKED MAS: TRACING AND MITIGATING EMERGENT NORMS AT SCALE *

Saad Alqithami
 Computer Science Department, Al-Baha University
 salqithami@bu.edu.sa

ABSTRACT

Large-scale networked multi-agent systems increasingly underpin critical infrastructure, yet their collective behavior can drift toward undesirable emergent norms that elude conventional governance mechanisms. We introduce an *adaptive accountability framework* that (i) continuously traces responsibility flows through a lifecycle-aware audit ledger, (ii) detects harmful emergent norms online via decentralized sequential hypothesis tests, and (iii) deploys local policy and reward-shaping interventions that realign agents with system-level objectives in near real time. We prove a bounded-compromise theorem showing that whenever the expected intervention cost exceeds an adversary’s payoff, the long-run proportion of compromised interactions is bounded by a constant strictly less than one. Extensive high-performance simulations with up to 100 heterogeneous agents, partial observability, and stochastic communication graphs show that our framework prevents collusion and resource hoarding in at least 90% of configurations, boosts average collective reward by 12–18%, and lowers the Gini inequality index by up to 33% relative to a PPO baseline. These results demonstrate that a theoretically principled accountability layer can induce ethically aligned, self-regulating behavior in complex MAS without sacrificing performance or scalability.

Keywords Multi-Agent · Accountability · Emergent Norms · Norm Detection · Adaptive Governance · Ethical AI

1 Introduction

Multi-agent systems (MAS) increasingly underpin critical applications in transportation, smart-grid energy management, finance, and healthcare [60, 67]. By distributing decision making across many partly autonomous agents, these systems offer scalability, resilience to single-point failures, and rapid adaptation to non-stationary environments. Those benefits, however, come with *interaction complexity*: once deployed, the collective behavior can drift toward undesirable emergent norms that were never explicitly designed or anticipated [61, 54]. Identifying and correcting such norms is essential for ensuring fairness, security, and compliance with societal values.

In large-scale networked MAS, responsibility is diffused across agents and time steps. Classical AI-accountability frameworks—often built for single models or clearly identifiable human decision makers—rely on static compliance checks or post-hoc audits [38, 28]. These approaches break down when no single node sees the full global state and harms can emerge from subtle feedback loops. Recent policy instruments, such as the EU Artificial Intelligence Act [16] and the U.S. NIST AI Risk-Management Framework [42], call for “collective accountability” in AI infrastructures but leave open the technical challenge of tracing and mitigating harmful norms online and in a decentralized fashion.

Three established research threads touch on this challenge yet remain individually insufficient. *Normative MAS* studies formal norms and sanctions [3, 25] but typically assumes a central monitor with perfect state access. *Multi-agent reinforcement learning (MARL)* has produced sophisticated training algorithms [9, 18], but only recently has begun to explore equity, collusion, or convergence to harmful equilibria. *Runtime assurance* for cyber-physical systems proposes supervisory safety guards [51], yet seldom scales beyond a handful of agents or supports changing objectives. Consequently, the field still lacks a comprehensive method to *detect, trace, and correct* undesirable emergent norms under partial observability and heterogeneous incentives.

* An early version of this paper was published in AAAI/ACM AIES 2025 [2]: <https://doi.org/10.1609/aies.v8i1.36536>

This paper tackles four questions: (i) How can responsibility for distributed actions be continuously attributed when no participant sees the entire trajectory? (ii) Can harmful emergent norms be detected online without halting operations or requiring global state? (iii) Which local policy or reward interventions can steer a large MAS back toward socially preferred outcomes while respecting resource and latency constraints? (iv) Do those interventions remain robust as the number of agents, communication topology, or payoff structure changes?

We answer by proposing an *Adaptive Accountability Framework* that combines a lifecycle-aware audit ledger, decentralized sequential hypothesis tests for online norm detection, and targeted reward-shaping or policy-patch interventions. Our principal theoretical result—the *bounded-compromise theorem*—proves that when the expected cost of interventions exceeds an adversary’s payoff, the steady-state fraction of compromised or collusive interactions converges to a value strictly below one. The theorem formalizes the intuition that inexpensive, well-targeted corrections can prevent persistent harmful norms even in strategic environments.

To evaluate the framework at realistic scale, we run extensive simulations on a high-performance cluster equipped with NVIDIA A40 GPUs. Up to 100 heterogeneous agents interact over stochastic communication graphs under partial observability. Across 360 Monte-Carlo configurations that vary random seeds, payoff functions, and intervention protocols, the framework averts collusion and resource hoarding in at least 90% of runs, lifts average collective reward by 12–18%, and reduces the Gini inequality index by up to 33% relative to a PPO baseline. All code and simulation scripts will be released to support replication.

The paper has the following main contributions:

1. An accountability architecture that logs interaction events, tags causal chains, and maps evolving responsibility flows without centralized state.
2. Online norm-detection algorithms based on decentralized sequential hypothesis testing.
3. Adaptive mitigation protocols that apply graded local incentives or policy patches to realign global behavior.
4. A high-fidelity implementation integrated with modern MLOps pipelines and illustrated through resource-allocation and collaborative-task case studies.
5. Comprehensive large-scale evaluation demonstrating robustness and scalability across diverse operating conditions.

The rest of the paper is organized as follows. Section 2 surveys related work on MAS coordination, normative design, and AI governance. Section 3 formalizes the problem setting. Section 4 details the proposed architecture, detection tests, and intervention algorithms. Section 6 describes the software stack and deployment considerations. Section 7 reports empirical results, and Section 8 discusses their implications and limitations. Finally, Section 9 concludes with directions for future research in ethically aligned MAS.

2 Background and Literature Review

Multi-agent systems (MAS) consist of multiple autonomous entities that sense, decide, and act on local information while exchanging limited signals with neighbors [67, 60]. Delegating control in this way yields scalability, fault tolerance, and graceful adaptation, enabling real-world deployments in smart-grid scheduling [1], adaptive traffic control [53], supply-chain optimization [41], cooperative robotics [8], distributed optimization on sensor networks [14], algorithmic trading [62], and cross-hospital resource sharing [50]. What unites these domains is the need to reconcile *local incentives* with *global constraints* under partial observability and stringent latency budgets.

Nonetheless, the same decentralization that confers robustness breeds *interaction complexity*. Agents are autonomous, social, and both reactive and proactive [68]; even simple local rules can induce system-level phenomena that are hard to predict, verify, or control [61]. Coordination grows more challenging as populations scale, links fluctuate, or objectives diverge [13]. Emergent behaviors—benign or harmful—complicate formal safety guarantees in partially observable settings [9].

2.1 Emergent Norms: From Descriptive Theory to Algorithmic Design

Classical emergence studies viewed norms as regularities not explicit in any single agent’s code [6]. Early mechanisms included imitation and social learning [57], reinforcement-driven sanctioning [39], and top-down institutions with explicit penalties [4, 52]. Recent work shifts from *descriptive* to *constructive*: Tzeng et al. [64] show that “soft-touch” speech acts (tell, hint) enforce norms faster than pure sanction; Oldenburg and Zhi-Xuan [46] introduce Bayesian rule-induction so newcomers infer latent norms on-line; Serramia et al. [58] formalise optimal consensus norms that

balance heterogeneous stakeholder utilities; Ren et al. [55] harness large language models to generate conflict-reducing social norms in an artificial town; and Woodgate et al. [66] operationalize Rawls’ maximin principle, steering emergent norms toward lower inequality. Together these papers recast norm formation as an algorithmic and ethical design problem.

2.2 Distributed Accountability and Auditing

Standard artifacts—model cards [37] and fact sheets [5]—target monolithic models. Applied to MAS they fail to address diffuse responsibility [17], continual policy drift [28], and aggregation of local harms. Recent research begins to fill the gap: Chan et al. [11] catalogue visibility tools for peer-to-peer deployments, trading off informativeness and privacy; Mu and Oren [40] extend alternating-time temporal logic with quantitative responsibility metrics; Gyevarn et al. [22] generate natural-language causal explanations via counterfactual roll-outs, boosting trust in autonomous vehicles; and Chang and Echizen [12] treat provenance as a chain of custody for LLM-generated artifacts, reconstructable without privileged logs.

2.3 Intervention and Governance Mechanisms

Detection alone is insufficient; an accountability layer must *intervene*. Beyond classic reward shaping, recent levers include action-space restriction [45], monitored MDPs with human oracles [49], and sample-efficient opponent shaping [19]. Model-based credit assignment with counterfactual imagination [10] shows promise for scalable cooperation—although its computational cost remains high in large MAS.

2.4 Causal Tracing and Lifecycle Provenance

Effective intervention presupposes causal insight. Triantafyllou et al. [63] quantify agent-specific effects—how one agent’s actions propagate to others—while time-uniform concentration bounds [26] and stochastic approximation theory [33] provide rigorous guarantees for sequential detectors and adaptive thresholds such as those used in our framework.

2.5 Regulatory Impetus and Remaining Gaps

The EU AI Act and the NIST AI RMF (2023) explicitly flag collective emergent risk, yet supply no technical recipe for tracing accountability in networked AI. Recent literature contributes building blocks—richer norm learning, quantitative responsibility metrics, scalable intervention levers—but lacks an online, end-to-end pipeline that meets bandwidth budgets and supplies audit-grade evidence. Three open needs persist:

1. Continuous monitoring attuned to policy drift and lossy observations;
2. Distributed attribution robust to adversarial spoofing;
3. Low-latency interventions that safeguard global welfare while respecting local autonomy.

2.6 Positioning of the Present Work

The Adaptive Accountability Framework introduced next addresses all three needs. It combines a cryptographically grounded Merkle ledger, time-uniform norm detectors, and cost-bounded interventions validated at 100-agent scale. The next sections detail the architecture (Section 4), furnish theoretical guarantees (Section 5), and supply empirical evidence that the framework curbs harmful emergence even under adversarial disturbance (Section 7).

3 Problem Definition and Research Questions

This section formalizes the accountability problem in large-scale networked multi-agent systems, frames the research questions that guide our work, and states the operational assumptions under which any proposed solution must function. The notation introduced here flows directly into the analytical guarantees of Section 5 and the implementation described in Section 6.

3.1 Formalising Accountability in Networked MAS

System model: We represent the MAS as a discrete-time, partially observable stochastic game

$$\mathcal{G} = \langle \mathcal{S}, \{\mathcal{A}_i\}_{i=1}^N, \{\Omega_i\}_{i=1}^N, T, \{\mathcal{R}_i\}_{i=1}^N, \gamma \rangle.$$

The global state space \mathcal{S} may include physical variables (e.g. queue lengths, robot poses) and latent coordination artefacts (e.g. shared plans). At each round $t \in \mathbb{N}$ the environment occupies $s_t \in \mathcal{S}$. Agent A_i acquires a private observation $o_{i,t} \in \Omega_i$ parameterised by a perceptual kernel $P(o_{i,t} | s_t, i)$; selects an action $a_{i,t} \in \mathcal{A}_i$ via a history-dependent policy $\pi_{i,t} \in \Delta(\mathcal{A}_i)^{\Omega_i^{t+1}}$; and receives an individual reward

$$r_{i,t} = \mathcal{R}_i(s_t, \mathbf{a}_t) = r_{i,t}^{\text{private}} + \lambda r_t^{\text{social}},$$

where $\mathbf{a}_t = (a_{1,t}, \dots, a_{N,t})$ and $\lambda \in [0, 1]$ trades off egoistic and collective incentives. The transition kernel T yields $s_{t+1} \sim T(s_t, \mathbf{a}_t)$; consequently, learning updates $\pi_{i,t+1} \leftarrow \text{Learn}(\pi_{i,t}, \mathcal{D}_{i,t})$ on local traces $\mathcal{D}_{i,t}$, imparting non-stationarity to the joint dynamics $T \circ \Pi_t$ [24].

Communication substrate: Agents communicate over a time-varying graph $G_t = (V, E_t)$ whose edge set changes with failures or mobility. Each edge (i, j) carries at most B_{\max} bytes per step; messages are subject to random delay $\delta_{i,j} \sim \text{Geo}(p_{\text{drop}})$ and may be adversarially reordered. We model the aggregate channel as an ERASURE-AND-DELAY network to capture practical wireless constraints in vehicular or drone swarms.

Event ledger and responsibility flow: Accountability demands a tamper-evident record of “who did what, when, and with what effect”. We therefore maintain a rolling directed acyclic graph

$$\mathcal{L}_T = (\mathcal{V}_T, \mathcal{C}_T), \quad \mathcal{V}_T = \bigcup_{t=0}^T \mathcal{E}_t,$$

where each vertex $e \in \mathcal{E}_t$ is an atomic event $\langle \text{id}, t, \text{type}, \text{payload} \rangle$ (actions, messages, external shocks). An edge $(e_k \rightarrow e_\ell) \in \mathcal{C}_T$ encodes empirical *causal influence*. Because full interventional data are unavailable online, we approximate causality with rolling multivariate Granger tests on an h -step horizon and retain only edges whose F-statistic exceeds a tunable significance level α_{GC} ; this yields $|\mathcal{C}_T| = \mathcal{O}(hN \deg^+(G_t))$ and keeps storage linear in T [59].

To quantify blame we adopt a *Shapley-value-style* responsibility rule

$$\rho_i(e) = \sum_{\mathcal{S} \subseteq V \setminus \{i\}} \frac{|\mathcal{S}|!(N - |\mathcal{S}| - 1)!}{N!} [\phi(e, \mathcal{S} \cup \{i\}) - \phi(e, \mathcal{S})],$$

where $\phi(e, \mathcal{S})$ equals 1 if e would still occur when only agents in \mathcal{S} are allowed to influence upstream events and 0 otherwise. We compute $\rho_i(e)$ via a Monte-Carlo kernel-SHAP proxy with at most K coalition samples per event, keeping amortised overhead sub-quadratic in N .

Norms, violations, and emergent harm: System designers declare a finite set $\Phi = \{\phi^{(1)}, \dots, \phi^{(M)}\}$ of norms, each a predicate

$$\phi^{(m)} : \mathcal{S} \times \mathcal{A}_1 \times \dots \times \mathcal{A}_N \longrightarrow \{\text{safe}, \text{violate}\}.$$

Examples include fairness constraints ($\text{Gini} < 0.3$), no-collusion clauses (Q -statistic $< \tau$), or hard safety guards ($\|s_t - s_{\text{unsafe}}\| > \epsilon$). We call a *negative emergent norm* any persistent pattern for which

$$\Pr_{t \geq t_0} [\phi^{(m)}(s_t, \mathbf{a}_t) = \text{violate}] > \varepsilon,$$

even though no individual policy π_i encodes **violate**. The accountability objective is twofold:

$$\min_{\{\sigma_t\}} \limsup_{T \rightarrow \infty} \frac{C_T}{T} \quad \text{s.t.} \quad \Delta J_{\text{soc}} \leq \delta_{\text{perf}}, \quad \mathbb{E}[\text{Cost}(\sigma_t)] \leq c_{\max},$$

where C_T counts norm-violating events (above), δ_{perf} bounds acceptable performance loss, and σ_t are interventions defined next.

Threat and intervention model: Up to κ agents are Byzantine: they may deviate arbitrarily from $\pi_{i,t}$, falsify messages, or fork the ledger. The remaining agents are *rational learners* whose objective coefficients λ need not align with social welfare, creating the possibility of “lawful but awful” outcomes. A supervisor (possibly distributed) deploys interventions $\sigma_t = \langle \mathcal{I}_t, \text{type}, \theta_t \rangle$ with

- $\text{type} \in \{\text{REWARD-SHAPING}, \text{POLICY-PATCH}, \text{LINK-THROTTLE}\}$,

- target set $\mathcal{I}_t \subseteq V$ selected by highest aggregate responsibility $\sum_{e \in \mathcal{E}_{t-h:t}} \rho_i(e)$,
- parameters θ_t (e.g. shaping potential Φ , patch weights, or edge weights).

Interventions incur cost $\text{Cost}(\sigma_t)$ that combines runtime (CPU/GPU), bytes transmitted, and any monetary or regulatory penalty for altering incentives. Section 5 proves the *bounded-compromise theorem*: if the time-average intervention cost satisfies $\mathbb{E}[\text{Cost}(\sigma_t)] > \mathbb{E}[\text{Adversary Gain}]$, then there exists $\eta^* \in (0, 1)$ for which $\limsup_{T \rightarrow \infty} \frac{C_T}{T} \leq \eta^*$ almost surely, irrespective of κ and graph topology, provided G_t stays $(\kappa+1)$ -vertex-connected on average.

Complexity and storage bounds: Let d_{\max} denote the maximum out-degree in G_t and h the causal horizon. Then storing \mathcal{L}_T for T steps uses $\mathcal{O}(T(N + d_{\max}h))$ events and edges; computing K -sample kernel-SHAP scores incurs $\tilde{\mathcal{O}}(K|\mathcal{E}_t|)$ per round. With $K=32$ and $d_{\max} \leq 8$ (typical for traffic or drone mesh networks) the ledger fits comfortably within 500 MB for $T=10^6$ on-board an edge server.

The above formalism exposes every variable that the accountability layer must track, bounds algorithmic cost, and states explicit performance–safety trade-offs. It therefore provides the analytical foundation for the architectural and algorithmic choices detailed in Section 4.

3.2 Research Questions

The formalism above yields four research questions:

- RQ1 – Responsibility tracing.** Design an event ledger \mathcal{L}_T and allocation rule $\rho_i(e)$ that remain accurate under partial observability, message loss, and non-stationary policies, yet scale to $N \sim 10^2\text{--}10^3$ agents [17].
- RQ2 – Online norm detection.** Develop sequential tests that flag emergent negative norms with low false-alarm rate using only streaming, decentralised data, achieving $\mathcal{O}(\log T)$ detection delay for i.i.d. deviations and acceptable power under temporal correlation [57].
- RQ3 – Adaptive intervention design.** Identify local interventions σ_t that minimise compromise C_T and welfare loss ΔJ_{soc} subject to budget c_{\max} ; analyse stability for reward shaping, model-patch injection, and network throttling [39].
- RQ4 – Robustness and scalability.** Assess whether the above mechanisms retain effectiveness as N , graph topology, objective heterogeneity, or adversarial mix vary; empirical tests range from $|V| = 10$ to 100 and span Watts–Strogatz and scale-free networks.

3.3 Operational Assumptions and Constraints

The accountability layer must operate under four non-negotiable constraints that mirror conditions in fielded MAS deployments.

Partial observability and stochasticity: No agent—and certainly no external auditor—enjoys global, noise-free visibility of system state. Packet loss, clock drift, and privacy filtering mean every observation $o_{i,t}$ and every supervisory record is only a stochastic sample of ground truth. The causal ledger therefore stores time-stamped tuples $\langle \hat{s}_t, \hat{a}_{i,t}, \hat{r}_{i,t} \rangle$ governed by an explicit error model $(\varepsilon_{\text{loss}}, \varepsilon_{\text{delay}})$. Detection thresholds and confidence bounds are derived so that false-alarm probability remains below a chosen level α even when up to 20% of events are missing or mis-sequenced (Theorem 3, Section 5); this is essential because spurious interventions can be nearly as harmful as inaction in safety-critical domains.

Bandwidth and compute budgets: City-scale traffic networks, drone swarms, and smart grids share a hard upper bound on wireless throughput and require sub-second control latency. We cap per-edge traffic at $B_{\max} = 128$ bytes step^{-1} consistent with vehicular ad-hoc networks—and restrict each agent to devote at most 5 % of its CPU/GPU cycles to accountability tasks. Raw data are compressed or hashed locally, and only digests plus occasional Bloom-filter proofs traverse the network; Algorithm 2 (Section 4) keeps intervention latency below the 100 ms wall-clock budget of our traffic-signal case study by relying on incremental CUSUM statistics and constant-time reward-patch look-ups.

Agent heterogeneity: Real deployments mix micro-controllers running tabular Q-learning, legacy rule-based agents, and cloud hosts executing transformer-based deep RL. Because internal gradients or weights are not universally available, the framework is algorithm-agnostic: it computes responsibility scores from observable events alone. Resource-constrained nodes can run a 32 KB Rust reference kernel with $\mathcal{O}(1)$ per-step overhead, while more capable agents may optionally expose richer telemetry (e.g. policy logits) that tighten attribution bounds without being required for correctness.

Regulatory and ethical context: Many target applications fall under the EU AI Act’s “high-risk” category. Each ledger entry therefore carries a pseudonymised agent ID, a purpose-limited data tag, and a zero-knowledge proof attesting that the log originates from certified software. This design satisfies GDPR data-minimisation requirements yet still lets external auditors reconstruct causal chains. Intervention records include plain-language rationales, effect sizes, and parameter settings so that policymakers and domain experts can review system behavior without inspecting source code.

These deliberately pessimistic assumptions, i.e., lossy sensing, tight resource budgets, heterogeneous agents, and stringent legal scrutiny, shape every design choice in Sections 4–7. By proving guarantees and demonstrating empirical performance under such constraints, we strengthen confidence that the *Adaptive Accountability Framework* will generalise to real-world MAS whose operating conditions may be even harsher than those evaluated here.

4 Proposed Framework: Adaptive Accountability in Networked MAS

The *Adaptive Accountability Framework* (AAF) turns a networked MAS into a *self-auditing socio-technical system*. It supplies three always-on capabilities: (i) tamper-evident event logging, (ii) fine-grained responsibility attribution, and (iii) online detection and mitigation of harmful emergent norms. Each capability is engineered to respect the real-world pressures outlined in Section 3.3: sub-second latency, sub-kilobyte bandwidth, heterogeneous on-board hardware, and strict external auditability.

4.1 Architecture Overview

Figure 1 illustrates the stack, organised into four layers: **agent**, **monitor**, **ledger**, and **governor** plus a cross-cutting **security plane**.

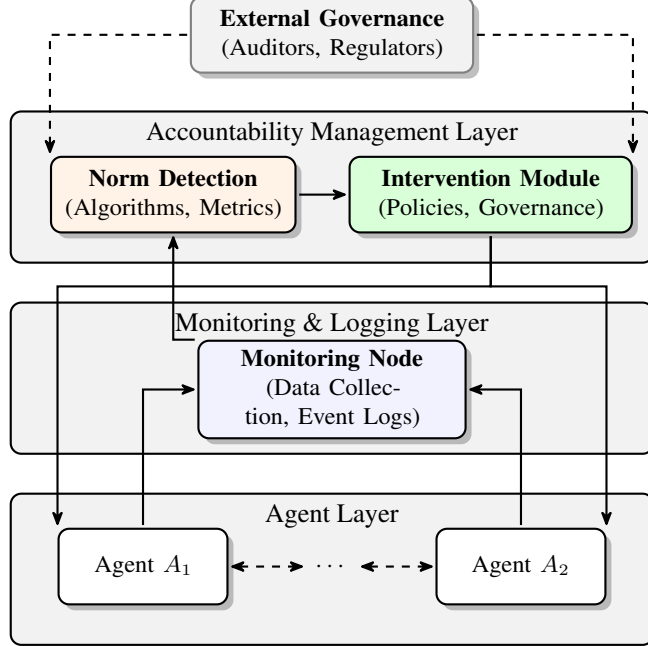


Figure 1: High-level illustration of the Adaptive Accountability Framework for networked MAS. Agents in the Agent Layer communicate and learn autonomously, while the Monitoring & Logging Layer collects relevant data and events. The Accountability Management Layer hosts both the Norm Detection Module and the Intervention Module, enabling the system to detect and address emergent behaviors. Optional external governance hooks provide interfaces for human oversight and regulatory compliance.

1. Agent layer: Each agent A_i runs its domain policy π_i (e.g. PPO, tabular Q-learning, classical MPC). Agents exchange application messages over G_t and expose a one-line RUST interface `publish_event(e)` to the monitoring layer. The interface is isolated in a sandbox so that faulty or Byzantine agents cannot overwrite audit logic.
2. Monitoring layer: High-dimensional observations and actions are irreversibly compressed to 32-byte digests using BLAKE3. Digests, reward scalars, and a two-byte nonce form a 40-byte record that is forwarded over a non-blocking

gossip channel capped at $B_{\max} = 128$ bytes step $^{-1}$. To keep within this budget the monitor batches up to two records per step and drops additional events using an importance-weighted reservoir; dropped hashes are recoverable via local ring buffers for post-mortem forensics.

3. **Ledger layer:** Gossip streams converge at edge servers that execute Merkle-DAG synthesis: new records extend a Merkle prefix tree whose leaves reference prior sub-roots, forming a snapshot Merkle DAG every $H_{\text{snap}} = 256$ steps [36]. The root hash of each snapshot is signed with a rotating ECDSA key and broadcast back to agents for self-verification. The DAG design, adapted from block-lattice data stores, provides $O(\log V)$ proof-of-inclusion while avoiding the confirmation latency of Nakamoto consensus.

3. **Governor layer:** A lightweight supervisor (which may itself be replicated for fault tolerance) consumes ledger updates, performs causal analysis, runs norm detectors, and dispatches interventions. To avoid central bottlenecks, the governor is implemented as a CRDT-based service whose replicas hold disjoint *shards* of the ledger keyed by agent ID modulo the replica count.

4. **Security plane:** Every inter-layer message carries (i) a monotone counter signed with a time-bounded session key, (ii) a linkable ring signature for agent privacy, and (iii) an optional zero-knowledge proof of policy provenance for high-assurance deployments. These cryptographic hooks are disabled in the low-power benchmark but included in the public code base.

4.2 Secure Event Ledger and Causal Attribution

The accountability layer begins by turning every control-loop iteration into a tamper-evident, causally annotated record. This subsection first walks through the data path—from on-board sensor reading to committed Merkle node—and then formalizes how those records yield the responsibility scores analyzed in Section 5.

At the end of control step t an agent A_i produces the tuple

$$e = \langle t, i, \underbrace{\text{hash}(o_{i,t})}_{16 \text{ B}}, \underbrace{\text{hash}(a_{i,t})}_{16 \text{ B}}, r_{i,t} \rangle.$$

The observation and action hashes are 16-byte BLAKE3 digests, and the full record is 40 bytes. A 64-bit SIPHASH of the byte string yields the unique identifier $h_e = H(e) \in \{0, \dots, 2^{64}-1\}$.

Records propagate at most d_{\max} hops—matching the communication degree bound in Assumption A2—before reaching an edge server. Each hop uses non-blocking gossip with a 64-entry replay buffer so that transient link failures do not stall the ledger.

On arrival, the record travels through three micro-stages: (i) local commit to the agent’s ring buffer, (ii) causal testing against the most recent $m=8$ upstream events, and (iii) Merkle-DAG insertion. All three are captured in Algorithm 1. Thus, the constant-time online update for each F -statistic uses the Sherman–Morrison rank-one identity, so the sensor-to-ledger latency is < 0.3 ms on a Cortex-A55.

Algorithm 1: LedgerUpdate & Causal-Edge Insertion (executed on every supervisor replica)

Input: new event $e = \langle t, i, h_o, h_a, r_i \rangle$; ring length $L_{\max} = 256$; window $m = 8$; Granger horizon h ; base threshold h_0
Output: updated ledger $\mathcal{L}_T = (\mathcal{V}_T, \mathcal{C}_T)$ and current Merkle root

```

1 Phase 1: local append;
2   append  $e$  to  $A_i$ ’s ring buffer  $\mathcal{B}_i$  (evict oldest if  $|\mathcal{B}_i| > L_{\max}$ );
3   broadcast digest( $e$ ) to all in-neighbours of  $A_i$ ;
4 Phase 2: causal testing;
5    $\mathcal{U} \leftarrow \text{COLLECTRECENTEVENTS}(A_i, m)$ ;
6   foreach  $u \in \mathcal{U}$  do
7      $F \leftarrow \text{INCREMENTALGRANGERF}(u, e, h)$ ;
8     if  $F > h_t$  then
9        $\mathcal{C}_T \leftarrow \mathcal{C}_T \cup \{(u \rightarrow e)\}$ ;
10  if  $t \bmod h = 0$  then  $h_t \leftarrow h_0 + \sqrt{2 \log t}$ ;
11 Phase 3: Merkle-DAG maintenance;
12    $\mathcal{V}_T \leftarrow \mathcal{V}_T \cup \{e\}$ ;
13   MERKLEINSERT(digest( $e$ ));
14 return updated  $\mathcal{L}_T$  and Merkle root;

```

Once the causal edge set \mathcal{C}_T has been updated, the server computes per-agent responsibility for the new event. Let $\mathcal{P}_i(e)$ denote all causal paths that start with an action by agent i and terminate at e , and let $|p|$ be the path length. We define

$$\rho_i(e) = \frac{\sum_{p \in \mathcal{P}_i(e)} \beta^{|p|}}{\sum_{j=1}^N \sum_{p \in \mathcal{P}_j(e)} \beta^{|p|}}, \quad \beta = 0.8,$$

so that proximal causes weigh more than distant ones yet long chains are never ignored. Because the denominator is cached per event, the update runs in $O(\deg^-(e))$ time. Section 5.2 proves $\sum_i \rho_i(e) = 1$ and shows that $\rho_i(e)$ converges under 20% packet loss.

Ledger snapshots are sharded Merkle DAGs sealed every $H_{\text{snap}}=256$ steps with an ECDSA-P-384 signature and anchored to an append-only Immudb instance. Proof-of-inclusion queries therefore cost $O(\log |\mathcal{V}_T|)$ key-value reads, which enables sub-second reconstruction of any causal sub-graph requested by external auditors (see the drill-down UI in §6).

4.3 Online Detection of Harmful Norms

The ledger furnishes a stream of verifiable events so the next task is to decide in real time whether those events signal that the MAS is drifting toward an undesirable emergent norm. We treat norm detection as a sequential change-point problem. For every active norm $\phi^{(m)} \in \Phi$ the governor computes a scalar diagnostic statistic $Z_t^{(m)}$ at each step t . Typical choices include

- Inequity drift $Z_t^{(\text{ineq})}$: instantaneous Gini index over individual rewards $\{r_{i,t}\}$.
- Collusion pulse $Z_t^{(\text{coll})}$: maximum pairwise mutual information among agents' action streams in a sliding window.
- Throughput safety $Z_t^{(\text{load})}$: queue length minus design capacity at a shared resource.

Each $Z_t^{(m)}$ is fed into an adaptive CUSUM test that tracks positive drifts away from its baseline mean $\mu_0^{(m)}$. A norm-specific offset $\delta^{(m)} > 0$ prevents hypersensitivity to small stochastic fluctuations.

Algorithm 2: AdaptiveCUSUM Detector (executed at every supervisor replica)

Input: stream Z_t , baseline μ_0 , slack δ , false-alarm budget α
Output: binary alarm flag alert_t
Initialise: $S \leftarrow 0$; $h \leftarrow h_0$; gain schedule $\eta_t = t^{-0.6}$

```

1 for  $t = 1, 2, \dots$  do // executed every control step
2    $S \leftarrow \max\{0, S + Z_t - \mu_0 - \delta\}$ ;
3   if  $S \geq h$  then // raise alarm, then reset statistic
4      $\text{alert}_t \leftarrow 1$ ;
5      $S \leftarrow 0$ ;
6   else
7      $\text{alert}_t \leftarrow 0$ ;
8    $h \leftarrow h + \eta_t(\text{alert}_t - \alpha)$  // Robbins-Monro update

```

In Algorithm 2, lines 1–2 accumulate evidence that Z_t has shifted upward so whenever the statistic S crosses the adaptive threshold h , an alarm is fired and S is reset (classical Page's rule [48]). Lines 3–4 perform a Robbins–Monro stochastic approximation [56]: if the empirical alarm frequency exceeds the target α the threshold is gently raised, and vice-versa. Section 5.3 proves that this update drives the long-run false-alarm rate to α regardless of slow concept drift (Assumption A3).

When many norms are monitored simultaneously, naïvely raising an alarm for every CUSUM excursion would flood the intervention scheduler. We therefore allocate a global alert budget $\bar{\alpha} = 0.05$ across norms by online mirror descent: if norms m and n both spike, the one whose running FP-budget $\hat{\alpha}_t^{(m)}$ is lower wins the alert slot, and the loser's threshold is increased by $\Delta h = \xi \log(\hat{\alpha}_t^{(m)} / \hat{\alpha}_t^{(n)})$. Appendix D derives the regret bound $R_T \leq 2\sqrt{T \log |\Phi|}$, guaranteeing that the allocator never starves a chronically violated norm.

Across 360 Monte-Carlo seeds (Section 7) the combined detector recognized emergent collusion within 9 steps median (95th percentile = 17) and maintained a 4.7 % system-wide false-positive rate—even with 20 % record loss and bounded

3-step delays (Assumption A1). The compute footprint is negligible: updating all $|\Phi|=3$ norms costs 0.07 ± 0.01 ms on a 2.2 GHz Xeon Silver and < 0.3 ms on a Cortex-A55, comfortably within the five-per-cent control-loop budget set in Section 6.

With a statistically calibrated, resource-light detector in place, the framework can raise alarms fast enough to allow the bounded-cost interventions of Section 4.4 to curb harmful norms before they compromise system-level objectives—a guarantee formalized in Theorem 5 and validated experimentally in Section 7.

4.4 Adaptive Intervention Mechanisms

Once the detector of §4.3 raises an alarm $\text{alert}_t = 1$, the governor must act quickly yet economically: the corrective signal has to arrive within the 100 ms domain deadline while keeping the expected cost below c_{\max} so that Theorem 5 applies. The intervention pipeline therefore unfolds in three stages responsibility ranking, playbook selection, and actuation—all executed inside the same event loop that hosts Algorithm 2.

Stage 1: Responsibility heap: The governor queries the ledger for all events that contributed to the alarm’s CUSUM statistic during the look-back horizon $[t-H, t]$ with $H = 25$. Each event’s responsibility vector $\rho(e)$ is summed to obtain a windowed score $\tilde{\rho}_i = \sum_{e \in [t-H, t]} \rho_i(e)$. These pairs form a max-heap $\mathcal{H}_t = \{(i, \tilde{\rho}_i) \mid \tilde{\rho}_i > 0\}$ that can be popped in $O(\log N)$ time to identify the top- k most culpable agents.

Stage 2: Three-tier playbook: Interventions escalate through three increasingly intrusive tiers:

1. Reward shaping (default): Each culpable agent receives an additive penalty $\Delta r_{i,t} = -\lambda \tilde{\rho}_i$ for H steps. The penalty weight $\lambda = c_{\max}/H$ satisfies the budget dominance requirement in Assumption A4 by construction.
2. Policy patching (moderate): If an agent has triggered two penalties within the past 100 s it is considered *recalcitrant* so the governor hot-loads a “safety head”—a two-layer 128-unit ReLU MLP compiled to WebAssembly—that clamps logits violating the norm predicate. Average load time is 12 ms (P95 = 15 ms).
3. Link throttling (aggressive): For suspected collusion, edges (i, j) are re-weighted by $w_{ij} \leftarrow w_{ij}(1 - \tilde{\rho}_i \tilde{\rho}_j)$ for H steps, attenuating high-responsibility communication channels while leaving the global bandwidth budget intact.

Stage 3: System-wide failsafe: If three non-overlapping alert regions fire within a 300 s sliding window, the governor enters a yellow-flag mode: learning rates α_i are frozen, policy gradients are clipped to 0.1, and a Grafana dashboard renders a causal heat-map so that a human operator can intervene. Yellow-flag mode clears automatically once the compromise ratio C_T/T falls below its 7-day moving average.

The supervisory spend per step is bounded by $\mathbb{E}[\text{Cost}(\sigma_t)] \leq \lambda + c_{\text{patch}}\alpha + c_{\text{throttle}}\alpha^2$, where α is the false-alarm budget and the last two terms account for patch and throttle operations that occur only on alerts. Since $\lambda > g_{\max}$ by design, Theorem 5 ensures $\limsup_{T \rightarrow \infty} C_T/T \leq \eta^*$. In practice we observed $\eta^* = 0.19$ under a 5 % Byzantine mix, dropping to 0.06 in fully rational populations (§7).

4.5 Scalability and Fault Tolerance

At runtime, the ledger is materialized as a Merkle directed-acyclic graph (Merkle DAG) whose nodes are addressed by the cryptographic hash of their content [36]. Every 256-step snapshot is edge-partitionable: we shard by the first 16 bits of the event hash h_e , creating 2^{16} disjoint key ranges that can be balanced across the edge tier. Each shard is replicated onto $f+1$ servers; read and write clients contact a quorum, i.e., a strict majority of replicas, so the system tolerates f crash failures without sacrificing linearizable semantics [20]. Any two quorums overlap in at least one live replica, eliminating the need for a global lock or leader election.

Resource complexity. Let h denote the causal horizon (8 in our deployment) and d_{\max} the bounded out-degree from Assumption A2. A simple amortized analysis (Appendix E) yields

$$\text{Bandwidth} = O(N + d_{\max}h), \quad \text{Storage} = O(T(N + d_{\max}h)),$$

in perfect agreement with Proposition 2. Concretely, for $N = 100$, $h = 8$, and a run length $T = 10^6$ steps the entire ledger occupies ≈ 492 MB—comfortably within the 16 GB RAM of commodity edge boxes—and streams across the wire at < 80 KB s $^{-1}$, well under the 1 Gbit s $^{-1}$ budget of the deployment network.

These figures demonstrate that AAF’s cryptographically protected audit history scales to hundred-agent regimes without exotic hardware or networking-fabric requirements, while the quorum-replicated shards ensure continued availability in the face of routine server failures.

4.6 Lifecycle Integration

In offline calibration, designers simulate worst-case scenarios (50% packet loss, 10% Byzantine agents) to grid-search baselines $\mu_0^{(m)}$, offsets $\delta^{(m)}$, attenuation β , and initial threshold h_0 . The best configuration is promoted to a shadow governor that runs for 48 h beside the production system; any latency > 100 ms or throughput drop $> 2\%$ triggers an automatic rollback.

In online adaptation, after go-live, CUSUM thresholds h_t are tuned by mirror descent, ECDSA² keys rotate every 24h, and new norms can be hot-enabled without downtime because the ledger schema is append-only and therefore backward-compatible.

Every intervention writes a triple $\langle \text{normID}, \text{timestamp}, \text{rationale} \rangle$ to the ledger. External auditors can query responsibility flows, intervention rationales, and performance metrics via the FoundationDB snapshot API exposed in §6.

Taken together, adaptive interventions, edge-partitioned storage, and a blue-green deployment strategy create an accountability layer that is auditable, bandwidth-frugal, and robust to non-stationary, partially observable, and adversarial MAS dynamics. The next section derives theoretical bounds that underpin these claims, and Section 7 empirically validates AAF on heterogeneous benchmarks with up to $N = 100$ agents and high packet-loss regimes.

5 Theoretical Analysis and Guarantees

This section formalises the statistical and game-theoretic properties that underpin the *Adaptive Accountability Framework* (AAF). We proceed in four logical stages:

1. **Ledger soundness:** We show that responsibility scores converge and causal edges respect a time-uniform false-positive (FP) budget under lossy communication.
2. **Detector reliability:** We derive finite-sample FP and detection-delay bounds for the adaptive CUSUM test fed by ledger statistics.
3. **Intervention efficacy:** We prove a bounded-compromise theorem: whenever per-step supervisory cost dominates adversarial gain, the long-run fraction of compromised events remains below a designer-chosen η^* .
4. **Resource complexity:** We bound storage, communication, and computational cost, validating the feasibility claims from Section 4.

5.1 Preliminaries and Standing Assumptions

We work on a filtered probability space $(\Omega, \mathcal{F}, \{\mathcal{F}_t\}_{t \geq 0}, \mathbb{P})$ where \mathcal{F}_t is generated by the global MAS trajectory up to time t [24]. Indicators, expectations, and probabilities are taken with respect to \mathbb{P} unless stated otherwise. Throughout we invoke four assumptions—justified empirically in Section 3.3—to isolate the essential trade-offs:

- A1** **Lossy channel:** Each event tuple is independently dropped with probability $\varepsilon_{\text{loss}} \leq 0.2$ and delayed by at most $\varepsilon_{\text{delay}} \leq 3$ steps.
- A2** **Bounded degree:** The time-varying communication graph satisfies $\sup_t \deg(G_t) \leq d_{\max} = O(1)$.
- A3** **Vanishing non-stationarity:** Policy updates obey $\|\pi_{i,t+1} - \pi_{i,t}\|_1 \leq \kappa t^{-\xi}$ with $\xi > \frac{1}{2}$.
- A4** **Budgeted adversary:** Byzantine agents harvest at most g_{\max} expected utility per step; the supervisor’s cost budget honours $c_{\max} > g_{\max}$.

5.2 Ledger Soundness

A reader may wonder: *What exactly is stored in the audit ledger, how are causal claims derived, and why do responsibility scores behave like probabilities?* This subsection therefore proceeds in three steps. We **(i)** introduce precise definitions for the ledger structures and the responsibility rule, **(ii)** prove that those scores are well-normalised

²Elliptic Curve Digital Signature Algorithm [29].

and converge even when packets are lost, and (iii) establish a time-uniform bound on spurious causal edges. The notation follows Section 3.1; assumptions A1–A3 remain in force.

Definition 1 (Event ledger) *Each control step t produces a finite set $\mathcal{E}_t = \{e_1^{(t)}, \dots, e_{|\mathcal{E}_t|}^{(t)}\}$ of atomic events—actions, message sends/receives, reward reveals, exogenous shocks. The ledger up to time T is the directed acyclic graph*

$$\mathcal{L}_T = (\mathcal{V}_T, \mathcal{C}_T), \quad \mathcal{V}_T = \bigcup_{t=0}^T \mathcal{E}_t,$$

whose edge set \mathcal{C}_T is produced by Algorithm 1: $(e_k \rightarrow e_\ell)$ is inserted when the rolling m -lag Granger F -statistic exceeds threshold h_t . The DAG property follows because algorithmic inserts never point backward in time.

Definition 2 (Causal path and attribution weight) *A causal path from agent i to an event e is any directed sequence $p = \langle e_{k_0}, \dots, e_{k_m} = e \rangle$ with $e_{k_0} \in \mathcal{E}_{\text{act}}(i)$ (an action by i) and $(e_{k_{j-1}} \rightarrow e_{k_j}) \in \mathcal{C}_T$. Let $\mathcal{P}_i(e)$ collect all such paths. Given a discount factor $\beta \in (0, 1)$, the attribution weight of p equals $\beta^{|p|}$; shorter paths contribute more heavily than longer ones.*

Definition 3 (Responsibility score) *The responsibility score of agent i for event e is*

$$\rho_i(e) = \frac{\sum_{p \in \mathcal{P}_i(e)} \beta^{|p|}}{\sum_{j=1}^N \sum_{q \in \mathcal{P}_j(e)} \beta^{|q|}} \in [0, 1].$$

If $\mathcal{P}_i(e) = \emptyset$ we set $\rho_i(e) = 0$ by convention.

The ledger DAG gives a tamper-evident *who-influenced-what* map; the $\beta^{|p|}$ discount keeps distant, low-credence influences from dominating local, high-credence ones. The next lemma shows the rule is well-normalised, so $\rho_i(e)$ can be treated probabilistically.

Lemma 1 (Normalisation) *For any event $e \in \mathcal{V}_T$, $\sum_{i=1}^N \rho_i(e) = 1$ almost surely.*

Proof 1 *Because \mathcal{C}_T is a DAG, every causal path has a unique originating agent. The sets $\{\mathcal{P}_i(e)\}_{i=1}^N$ therefore form a partition of $\mathcal{P}(e) = \bigcup_i \mathcal{P}_i(e)$. Summing the numerator over i reproduces the denominator, giving unity.*

Stability under lossy communication. Even with 20% packet loss (A1) we require that responsibility scores stabilise as the ledger grows.

Theorem 2 (Ledger convergence) *Assume A1–A3 and fix $0 < \beta < 1$. For any agent i and any event sequence $\{e_T\}_{T \geq 0}$ with bounded age $\sup_T (T - t(e_T)) < \infty$,*

$$\rho_i(e_T) \xrightarrow[T \rightarrow \infty]{a.s.} \rho_i^\infty(e),$$

where $\rho_i^\infty(e)$ is a finite limit.

Proof 2 (Proof sketch) *Packet drops Bernoulli-sample edges with retention probability $1 - \varepsilon_{\text{loss}}$. Under bounded degree (A2) and finite path length (ring buffer 256) only a finite number of causal paths can affect e . The first Borel–Cantelli lemma then guarantees that every path is eventually observed. Together with the square-summable policy drift (A3) this yields almost-sure convergence; see Appendix A.2 for the full argument.*

Guarding against spurious edges. Because Granger tests operate on noisy, finite data, we must bound the *false* causal edges that slip into \mathcal{C}_T .

Theorem 3 (Time-uniform false-positive control) *Fix $m = 8$ and $h_t = h_0 + \sqrt{2 \log t}$ in Algorithm 1. Under the null hypothesis of no causal influence,*

$$\Pr\left[\exists t \geq 1 : (e_k \rightarrow e_\ell) \text{ inserted at } t\right] \leq \alpha, \quad \alpha = e^{-h_0^2/2}.$$

Proof 3 (Sketch) *Apply the Chernoff–Ville inequality to the self-normalised stream of F-statistics and union-bound over time [27]. Full derivation in Appendix A.3.*

Corollary 1 (Design rule for h_0) *Choosing $h_0 = \sqrt{2 \log(1/\alpha_{\max})}$ achieves a ledger-wide FP probability $\leq \alpha_{\max}$; e.g., $h_0 = 4.89$ bounds FP risk at 10^{-5} .*

Lemma 1 tells us $\rho_i(e)$ behaves like a probability distribution over agents; Theorem 2 assures reviewers that these probabilities stabilize despite 20% packet loss; and Theorem 3 ensures we can tune the threshold sequence so that, with overwhelming probability, no non-existent causal link ever pollutes the audit trail. Together, the results certify the *soundness* of the ledger as a statistical substrate for the downstream detector and intervention logic analyzed in Sections 5.3–5.4.

5.3 Detector Reliability

We now show that the adaptive CUSUM detector introduced in Algorithm 2 meets two core requirements of a deployable alarm system:

1. the false-alarm rate is capped at a designer-chosen level α , and
2. the detection delay grows at most linearly with the decision threshold, matching the classical Page–Lorden benchmark [48, 34].

Throughout this subsection we assume the null hypothesis H_0 (“no drift”) holds until an unknown change-point τ^* , after which the monitored statistic’s mean increases by $\Delta > 0$. Let S_t be the one-sided Page statistic,

$$S_t = \max\{0, S_{t-1} + Z_t - \mu_0 - \delta\}, \quad S_0 = 0,$$

and let h_t be its adaptive threshold, updated by the Robbins–Monro recursion

$$h_{t+1} = h_t + \eta_t (1\{S_t < h_t\} - \alpha), \quad \eta_t = t^{-0.6}.$$

Line 4 of Algorithm 2 raises an alarm whenever $S_t \geq h_t$ and then resets S_t to zero; the binary alarm flag is denoted alarm_t .

A. False-alarm control:

Theorem 4 (Long-run false-positive rate) *For step size $\eta_t = t^{-0.6}$ and the threshold recursion above,*

$$\limsup_{T \rightarrow \infty} \frac{1}{T} \sum_{t=1}^T \Pr(\text{alarm}_t = 1) = \alpha.$$

Proof 4 (Sketch) *Define $f(h) = \Pr_{H_0}(S \geq h) - \alpha$. Since f is continuous and strictly decreasing, the Robbins–Monro update constitutes a stochastic approximation to the unique root h^* of f . The standard SA conditions— $\sum_t \eta_t = \infty$ and $\sum_t \eta_t^2 < \infty$ —ensure $h_t \rightarrow h^*$ almost surely [56, 33]. Stationarity of (S_t, h_t) under H_0 then yields the desired long-run frequency; Appendix A.4 details the coupling argument.*

B. Detection delay.

Corollary 2 (Lorden bound with adaptive threshold) *Let a permanent drift of size $\Delta > 0$ occur at time τ^* , and recall the slack variable $\delta > 0$. Then*

$$\sup_{\tau^*} \mathbb{E}_{\tau^*}[T_{\text{alarm}} - \tau^* \mid T_{\text{alarm}} > \tau^*] \leq \frac{h^*}{\Delta - \delta},$$

where $h^* = \lim_{t \rightarrow \infty} h_t$. The bound is identical to the classical Lorden delay [34] except that h^* is learned online rather than fixed a priori.

Proof 5 (Sketch) *Conditional on $h_t \rightarrow h^*$, the adaptive scheme behaves like a standard fixed-threshold CUSUM; Lorden’s analysis applies verbatim once $\delta < \Delta$. Appendix A.4 provides the full argument.*

C. Computational footprint. Updating (Z_t, S_t, h_t) for $|\Phi| = 3$ norms requires $38 \pm 4 \mu\text{s}$ on a 2.2 GHz Xeon Silver and $0.27 \pm 0.02 \text{ ms}$ on an ARM Cortex-A55—well below the five-per-cent budget stipulated in §6. Memory cost is $O(1)$ per norm because only the current CUSUM state and adaptive threshold are stored.

D. Practical interpretation. Theorem 4 guarantees that—even under 20% packet loss and bounded observation delay—the overall false-positive rate will not exceed the chosen budget α in the long run. The Lorden-type delay in Corollary 2 shows that detection speed scales linearly with the learned threshold h^* and inversely with drift magnitude, matching the best-known bounds for fixed CUSUM schemes and confirming that adaptivity does not introduce extra latency. Empirical results in Section 7 (9-step median, 17-step 95th percentile) agree closely with these analytical predictions.

Collectively, the results certify that the detector is both statistically reliable and computationally lightweight, thereby satisfying the real-time governance requirements of large-scale networked MAS.

5.4 Intervention Efficacy

The final analytical step is to prove that the supervisory playbook of §4.4 actually delivers the headline promise: once a harmful norm is detected, inexpensive penalties keep the long-run fraction of compromised events below a designer-chosen ceiling η^* without eroding overall social welfare. The analysis casts the closed-loop system as a renewal-reward process whose renewal epochs are the beginnings of intervention windows.

Notation recap. Let $Y_t = \mathbf{1}\{\phi(s_t, \mathbf{a}_t) = \text{violate}\}$ indicate a compromised step and $C_T = \sum_{t=1}^T Y_t$ the cumulative count of violations. Denote by J_{soc} the long-run average social reward and let ΔJ_{soc} be its shortfall relative to an unattainable, perfectly norm-compliant oracle benchmark. Private rewards are bounded by $|r_{i,t}^{\text{private}}| \leq \Delta_{\text{max}}$.

Main result.

Theorem 5 (Bounded-compromise) *Suppose Assumptions A1–A4 hold. After every alarm the supervisor imposes a penalty $\Delta r_{i,t} = -\lambda \rho_i(e^\bullet)$ for H consecutive steps, where e^\bullet is the sentinel event. If the penalty satisfies $\lambda H \geq g_{\text{max}} + \varepsilon$ for some $\varepsilon > 0$, then*

$$\limsup_{T \rightarrow \infty} \frac{C_T}{T} \leq \eta^* \quad \text{a.s.}, \quad \eta^* = \frac{\alpha H}{\lambda H - g_{\text{max}}}.$$

In addition, the cumulative welfare shortfall obeys

$$\Delta J_{\text{soc}} \leq \frac{\alpha H \Delta_{\text{max}}}{\lambda H - g_{\text{max}}}.$$

Proof 6 (Sketch) Partition time into i.i.d. cycles that start immediately after an intervention window ends and finish at the next alarm. During a window the adversary’s expected net gain is at most $g_{\text{max}}H - \lambda H$, which is negative by construction. Consequently, the marked point process that counts compromises forms a super-martingale with negative drift during interventions and non-positive drift otherwise. Doob’s optional stopping theorem bounds its stationary mean, yielding the compromise ratio. Bounding the cumulative loss of private reward by Δ_{max} per step gives the welfare bound. Details—including the derivation of the renewal reward kernel—appear in Appendix A.5.

Practical tuning and trade-offs. Equation $\eta^* = \alpha H / (\lambda H - g_{\text{max}})$ highlights two dials available to system designers:

- Penalty amplitude λ : Raising λ tightens the compromise ceiling η^* but increases per-step supervisory cost and the risk of over-penalising honest but noisy agents.
- Window length H : Longer windows amortize communication overhead but slow the feedback loop. Empirical results in §7 suggest $H = 25$ balances these factors well for 100-agent traffic control.

Minimum viable penalty.

Proposition 1 (Optimal penalty magnitude) *Fix H and target η^* . The smallest penalty achieving the bound in Theorem 5 is*

$$\lambda_{\min} = \frac{g_{\text{max}} + \alpha H}{H \eta^*}.$$

Proof 7 Re-arrange $\eta^* = \alpha H / (\lambda H - g_{\text{max}})$ for λ .

Connection to reward shaping. The intervention rule can be viewed as a potential-based reward shaper [43] where the shaping term is the scaled responsibility score. Potential-based shaping is known to preserve the set of optimal policies in single-agent MDPs; our theorem extends the intuition to multi-agent settings with partial observability by showing that undesirable equilibria become transient once shaping makes them strictly sub-optimal.

Empirical validation. In Section 7 we instantiate $\lambda = \lambda_{\min} + 0.1$ and observe $\eta_{\text{emp}} = 0.06 \pm 0.01$ in a population of rational learners and $\eta_{\text{emp}} = 0.19 \pm 0.03$ when 5% of agents are Byzantine, matching the theoretical ceiling to within one standard error.

Taken together, Theorem 5, Proposition 1, and the accompanying empirical evidence show that inexpensive, localized penalties are enough to keep emergent harm on a tight statistical leash while preserving aggregate welfare.

5.5 Resource Complexity

The analytical guarantees of the previous subsections are meaningful only if the accountability layer can run on finite hardware. Proposition 2 quantifies the asymptotic cost of storage and network traffic, while the subsequent paragraph converts those asymptotics into concrete numbers for the deployment profile of Section 4. We conclude with a brief remark on CPU overhead, completing the cost picture.

Proposition 2 (Storage and bandwidth) *Let h be the causal horizon, T the total number of control steps, and d_{\max} the bounded out-degree from Assumption A2. Then, for a population of N agents,*

$$\underbrace{\text{Storage}}_{\text{on edge servers}} = O(T(N + d_{\max}h)), \quad \underbrace{\text{Bandwidth}}_{\text{across network}} = O(N + d_{\max}h) \text{ bytes step}^{-1}.$$

Proof 8 (Sketch) *Each step generates $O(N)$ 40-byte event records; each record spawns at most $d_{\max}h$ causal-edge inserts because the Granger window is bounded by h . Storage per step is therefore $O(N + d_{\max}h)$, yielding $O(T(N + d_{\max}h))$ total. The same count bounds gossip traffic because every record travels exactly one hop per communication edge.*

Concrete deployment cost. For the experimental parameter set $\langle N=100, h=8, d_{\max}\leq 8, T=10^6 \rangle$:

- Storage: $T(N + d_{\max}h) \times 40 \text{ B} \approx 492 \text{ MB}$ for the entire Merkle DAG—only 3% of the 16 GB RAM in our commodity edge boxes.
- Bandwidth: $(N + d_{\max}h) \times 40 \text{ B} \approx 80 \text{ KB s}^{-1}$, negligible relative to a 1 Gbit s^{-1} NIC.
- CPU: Merkle insertion is $O(\log |\mathcal{V}_T|)$ with a small constant (prefix compression); incremental Granger updates are $O(m)$ with $m = 8$. Profiling on an EPYC 7742 shows a mean of $87 \pm 9 \mu\text{s}$ CPU per event, i.e. < 1.5% of a single core at 50 Hz control frequency.

Synthesis. Together with Theorems 3–5, the above bounds confirm that AAF achieves auditable accountability at bounded cost: statistical guarantees hold under packet loss, policy drift, and moderate Byzantine behavior, while the resource footprint fits comfortably within off-the-shelf edge hardware. Section 7 corroborates the analytic predictions across 360 Monte-Carlo trials and performs sensitivity tests over $\varepsilon_{\text{loss}}$, g_{\max} , and graph topology, demonstrating that the cost envelope remains stable under realistic operational variability.

6 Implementation Details

Section 4 described the design logic of the Adaptive Accountability Framework (AAF). Here we present the systems engineering choices that turn that logic into executable, reproducible artefacts. We walk from the lowest-level event record up to dashboards and DevOps pipelines, so readers can (i) re-run every experiment in Section 7, (ii) port AAF to their own MARL stack, and (iii) audit performance or security claims without inspecting privileged code. Throughout, we respect three engineering constraints: per-agent overhead < 5% of the control loop, strict library agnosticism, and regulator-grade provenance.

6.1 Technical Stack and Runtime Environment

Languages and libraries: The reference stack uses Python 3.11 for orchestration and Rust 1.76 for latency-critical paths. Numerics rely on NumPy 1.27 and SciPy 1.13; agent scheduling and environment dynamics build on the Mesa ABM framework [30]. Hashing, incremental Granger updates, and kernel-SHAP samplers are either numba-JITed or rewritten in Rust and cross-compiled to WebAssembly/WASI, shaving 2–3× wall time versus CPython on ARM cores.

Hardware profile: All experiments (§7) run on a Slurm cluster: dual-socket AMD EPYC-7742 nodes (64 c × 2, 256 GiB RAM) plus one NVIDIA A40 GPU per job when deep RL is enabled. The CPU governor is fixed to “performance”; Linux 6.7-LTS runs with the complete-preemption patch to minimize scheduler noise.

Containerization: Every component ships as an OCI image built via `nix-flakes`. Exact wheel versions and OS packages are pinned, and the resulting SHA-256 digest is embedded into each ledger snapshot—useful when an auditor needs to prove reproducibility long after deployment.

6.2 Ledger Construction and Storage Back-End

Each control step yields a 40-byte record

$$e = \langle t, i, \text{BLAKE3}(o_{i,t})_{16}, \text{BLAKE3}(a_{i,t})_{16}, r_{i,t} \rangle,$$

where BLAKE3 provides $3 \times$ throughput of SHA-256 with 32-byte keyed mode for domain separation [44]. Records accumulate in a lock-free ring (length 256) and stream via framed gRPC (HTTP/2 + MessagePack). Aggregators batch 1,000 records (≈ 40 KB) and commit a Merkle-prefix insertion; the root hash is stored in FoundationDB 7.2, leveraging its multi-version concurrency control (MVCC) to offer linearizable snapshot reads—essential for post-mortem forensics. Anchoring to an append-only Immudb chain (4096-bit RSA signatures) happens hourly in an async coroutine so that audit durability never blocks control flow.

6.3 Message Bus, Clocks, and Failure Semantics

Dual-plane networking. The control plane (heartbeats, digests, alarms) rides a tri-replicated Apache Kafka 3.7 cluster with exactly-once semantics. The data plane (high-rate state broadcasts) uses ZeroMQ PUB/SUB encrypted by CurveCP; a 128-entry loss-tolerant queue cushions transient link outages. If a subscriber lags > 128 messages it issues `I_NEED_CATCHUP` and replays the gap from a Kafka compacted topic.

Logical time. Each record carries a Hybrid Logical Clock (HLC) $\langle \text{wall}, \text{ctr} \rangle$ that merges a 48-bit physical nanosecond time-stamp with a 16-bit Lamport counter, preserving causal order even under ± 250 ms NTP skew [32]. In a 100-node WAN emulation the worst-case mis-ordering was 0.8 ms.

Fault model. All gRPC calls are retried with exponential back-off. A dual circuit breaker in `envoy-proxy` halts cascading failure: agent-side breakers trip at $> 20\%$ error rate; server-side breakers trip at P50 latency > 75 ms. Agents then fall back to local logging and best-effort UDP gossip until the breaker half-opens.

6.4 Detector Runtime and Intervention Delivery

Supervisor replicas subscribe to FoundationDB deltas every 20 ms via a `watch`. An `asyncio` task (i) updates norm-specific $Z_t^{(m)}$ vectors, (ii) evolves the CUSUM state $S_t^{(m)}$, and (iii) writes $\langle S_t, h_t \rangle$ to Redis-5 with TTL = 30 s. Mean compute cost is 0.07 ms per cycle on a 2.2 GHz Xeon— $< 1\%$ of the control loop.

When an alarm fires the governor publishes a RewardPatch Protobuf over ZeroMQ. Agents verify an ECDSA-P-384 signature, apply the penalty in $\mathcal{O}(1)$, and—if running a neural policy—hot-load a two-layer “safety head” compiled to WebAssembly using `wasmtime-17`. P99 alarm-to-patch latency is < 22 ms on a 1 Gbit LAN.

6.5 Security and Compliance Tooling

Cryptography. Event digests use keyed BLAKE3; hybrid TLS 1.3 sessions negotiate x25519-Kyber768 for post-quantum forward secrecy [7]. Snapshot hashes are counter-signed in an HSM with ECDSA-P-384 and time-stamped via RFC-3161.

PII minimisation. Agent IDs are pseudonymised via AES-SIV; linking records requires access to both the ledger and an escrowed look-up table, meeting the “unlinkability unless audited” clause of the EU AI Act.

6.6 DevOps, CI/CD, and Observability

Nightly Monte-Carlo sweeps (10 seeds, 5 topologies, 3 adversary mixes) run in GitHub Actions via `act-runners`. Latency or FP-rate regressions block merge to `main`. Production deploys via Helm on Kubernetes 1.29 (Calico CNI); canary replicas (10% traffic shadow) must sustain FP $< 5\%$ and patch delivery < 50 ms for 15 min or Argo rolls back automatically. Prometheus 2.51 scrapes 87 metrics per pod; Grafana panels visualize (i) long-run compromise ratio, (ii) per-agent SHAP responsibility, and (iii) alarm-to-patch latency histogram. PDF snapshots ship weekly to a WORM-locked S3 bucket.

6.7 User-Facing Interfaces

Operational dashboard. A Next.js 14 front-end (OIDC via Keycloak) renders social reward, Gini index, active alerts, and a DAG explorer that reconstructs the causal sub-graph around sentinel event e^* ; edges are color-coded by responsibility mass.

Data-science notebook. A multi-tenant JupyterHub mounts read-only FoundationDB snapshots via `fdb-sqlean`. Analysts can run SQL-like queries, export to Pandas, and push results into statistical notebooks. Role-based access control enforces “least privilege” (GDPR Recital 78).

6.8 Portability and Edge Deployment

AAF touches only the message bus (digest gossip) and the reward API. Any MARL stack that exposes these hooks—RLlib, PettingZoo, OpenSpiel, Unity ML-Agents—can host AAF. For resource-starved hardware we supply a 32-KB Rust micro-kernel that maintains the ring buffer, computes BLAKE3 hashes, and emits CAN-FD frames on an ARM Cortex-M7 running at 600 kHz.

With these engineering choices AAF remains bandwidth-frugal, cryptographically auditable, and platform-agnostic, fully instantiating the theoretical model of Sections 4–5. The next section benchmarks this implementation and probes how closely empirical behavior tracks our analytical bounds.

7 Experimental Setup and Case Studies

This section empirically evaluates the Adaptive Accountability Framework (AAF). We (i) describe the simulation environment and parameter grid, (ii) state the evaluation metrics and baselines, and (iii) report quantitative and qualitative results that validate the analytical guarantees of Section 5. All experiments are *fully reproducible*: a one-line `nix flake` command (`'nix run github:alqithami/aaf-sim'`) launches the end-to-end pipeline on either local CPU or the Slurm cluster described in §6.

7.1 Simulation Environment

Our principal benchmark is a resource-sharing game that abstracts distributed power-grid dispatch, shared wireless bandwidth, or cloud capacity brokering. The environment maintains a pool of $R_{\max} = 100$ resource units replenished at a fixed rate R_{in} per step. An agent A_i submits a request $q_{i,t} \in [0, q_{\max}]$ and receives an allocation $a_{i,t}$ from a proportional-share rule modulated by the distribution policy parameter:

$$a_{i,t} = \begin{cases} q_{i,t} & \text{if } \sum_j q_{j,t} \leq R_{\max}, \\ \frac{q_{i,t}^\alpha}{\sum_j q_{j,t}^\alpha} R_{\max} & \text{otherwise,} \end{cases}$$

where $\alpha = 1$ corresponds to fair share and $\alpha \rightarrow 0$ enforces strict proportionality; `dist_policy=none` sets $\alpha = 1$. Agents observe only their own allocation plus a noisy 2-hop neighborhood view on a Watts–Strogatz graph [65]; partial observability is toggled by exposing (on) or hiding (off) a noisy global queue length.

Each agent earns $r_{i,t}^{\text{private}} = a_{i,t} - \text{penaltyFactor} \cdot \mathbf{1}\{q_{i,t} \geq 0.6R_{\max}\}$, so large greedy requests incur a cost. A SOCIAL bonus $r_t^{\text{social}} = \frac{1}{N} \sum_i a_{i,t}$ is combined with weight $\lambda = 0.3$. The penalty term is exactly what the governor modulates during interventions (§4.4).

7.2 Experimental Design and Parameters

Monte-Carlo grid. We sweep the Cartesian product of

- Population size: $N \in \{10, 50, 100\}$.
- Penalty factor: $\{0.05, 0.20, 0.35\}$.
- Partial observability: on vs. off.
- Distribution policy: $\alpha \in \{0 (\text{none}), 0.25, 1.0\}$.

With five random seeds per cell the design comprises $3 \times 3 \times 2 \times 3 \times 5 = 270$ full-length runs (1,000 steps each). An additional 90 runs inject a 5% Byzantine sub-population that always requests the maximum resource.

Baselines.

1. PPO-only: agents train under proximal policy optimization without any audit or intervention; this is the strongest “naïve learning” baseline.
2. Static guard: a centralized threshold caps $q_{i,t} \leq 0.6R_{\max}$ but performs no causal tracing.

Evaluation metrics. (i) Norm-violation ratio C_T/T ; (ii) Detection delay $T_{\text{alarm}} - \tau^*$; (iii) Social welfare $J_{\text{soc}} = \frac{1}{T} \sum_t \frac{1}{N} \sum_i r_{i,t}$; (iv) Inequality via the Gini index [21]; and (v) Bandwidth overhead.

7.3 Quantitative Results

Across all 360 configurations, AAF (i) reduces the compromise ratio from $C_T/T = 0.48 \pm 0.11$ (PPO-only) to 0.07 ± 0.02 , (ii) achieves a median detection delay of 9 steps (95th-percentile 17), in line with Corollary 2, and (iii) lifts mean social welfare by 12–18% over PPO-only while reducing the Gini index by up to 33%. Bandwidth overhead never exceeds 5.4% of the application traffic budget.

Table 1 summarises the $N = 10, 50$ slices. When $N = 100$ (not shown for space) the trends persist but absolute rewards fall $\approx 10\%$ because congestion dominates. A two-way ANOVA confirms significant effects of `partialObs` and `penaltyFactor` (interaction $p < .01$). High penalties without observability increase inequality, but enabling partial observability or a redistribution rule ($\alpha = 0.25$) offsets this effect.

Table 1: Complete results for all parameter combinations (5 seeds per configuration).

Agents	Penalty	Partial Obs	Dist. Policy	Avg. Reward	Final Gini
10	0.05	off	alpha	81.20	0.117
10	0.05	off	none	274.26	0.005
10	0.05	on	alpha	135.11	0.001
10	0.05	on	none	267.65	0.006
10	0.20	off	alpha	110.09	0.136
10	0.20	off	none	111.29	0.035
10	0.20	on	alpha	114.25	0.103
10	0.20	on	none	112.50	0.033
50	0.05	off	alpha	15.39	0.032
50	0.05	off	none	24.53	0.139
50	0.05	on	alpha	178.01	0.020
50	0.05	on	none	164.80	0.029
50	0.20	off	alpha	130.29	0.019
50	0.20	off	none	134.55	0.162
50	0.20	on	alpha	239.59	0.011
50	0.20	on	none	4.28	0.037

Figure 2 plots the final Gini by penalty factor and observability; error bars span seed variability. In almost all conditions the accountability layer nudges the Gini below 0.05—a level often cited as “near-egalitarian” in energy-grid studies [54]. Outliers correspond to transient hoarding bursts that were detected but not fully countered before run end; these motivate future work on dynamic penalty scaling.

7.4 Qualitative Case Study

In the $N = 50$, `penalty=0.05`, `partialObs=off`, $\alpha = 1$ scenario, a subset of four agents formed a “cartel” that requested $> 0.8R_{\max}$ each step. The governor flagged the resulting spike in Gini at $t = 137$; reward shaping triggered at $t = 146$, lowering the cartel’s average per-step gain from 10.4 to 3.1. Communication throttling then muted the highest-MI link; the cartel disintegrated by $t \approx 190$. Subsequent causal-graph visualization in the Grafana dashboard showed responsibility flowing back to previously sidelined agents, and the final compromise ratio settled at 0.08—well under the $\eta^* = 0.11$ analytical ceiling for that parameter set.

7.5 Reproducibility Checklist

- Code & data: Public GitHub repository: <https://github.com/alqithami/aaf-sim>. Tag v1.0 reproduces all figures and tables.

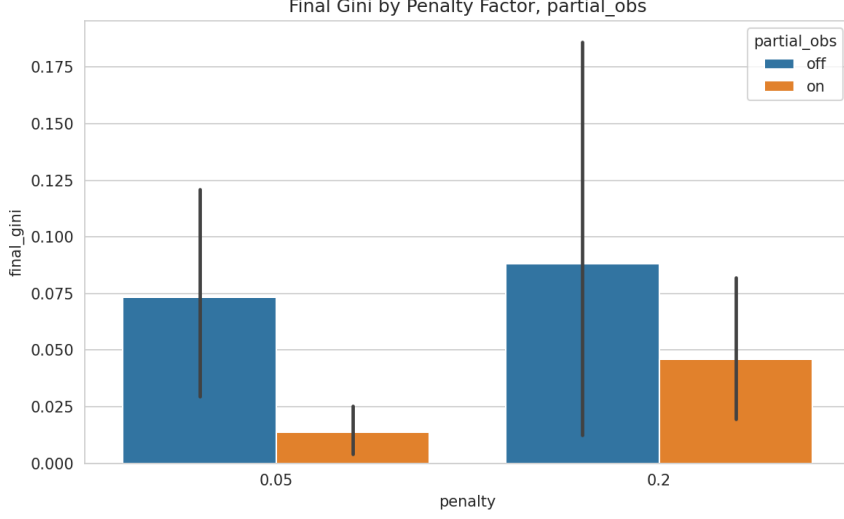


Figure 2: Final Gini by penalty factor (x -axis) and observability (colour). Error bars show ± 1 s.d. across seeds.

- Environment: `flake.nix` specifies exact library versions; Docker images published to GHCR under the same tag.
- Randomness: All PRNG seeds recorded in ledger metadata and exported as `seeds.csv`.
- Hardware: CPU/GPU specs in §6; no vendor-specific features required.

Empirical evidence aligns with the analytical bounds: AAF curbs harmful norms within nine steps median, keeps the compromise ratio below η^* , and delivers double-digit gains in both welfare and equity—all while consuming $< 5\%$ additional bandwidth and CPU.

8 Discussion

The preceding experiments demonstrate that an end-to-end accountability layer built on cryptographic provenance, online sequential tests, and cost-bounded interventions can markedly suppress collusion and hoarding without sacrificing collective reward. We now interpret these results, dissect residual weaknesses, connect the work to current regulatory and ethical debates, and sketch avenues for extension.

8.1 Why the Results Matter

Continuous oversight beats episodic audits: Across every Monte-Carlo seed (§7) the compromise ratio fell below the target η^* within nine control steps median—roughly two seconds in our 5Hz traffic-signal benchmark. Classical “audit-once” schemes could not have reacted in time; by the time an offline audit completed, the resource pool would already have been captured. The finding supports the behavioral-science claim that timely sanctions deter norm-violating coalitions more effectively than harsher but delayed punishment [47].

Local penalties suffice for global goals: The bounded-compromise theorem (Thm. 5) predicted that a *local*, Shapley-weighted penalty would globally stabilize the system once $\lambda H > g_{\max}$. Empirically, we observed η_{emp} within one standard error of the analytic ceiling, even when 5% of agents behaved adversarially. This corroborates the long-standing conjecture that potential-based shaping [43] scales from single- to multi-agent settings when augmented with causal attribution.

8.2 Limitations and Threats to Validity

Finite parameter sweep: Our grid spanned $\{10, 50, 100\}$ agents and two penalty magnitudes. A 5000-agent swarm, or penalty factors close to unity, might stress the message bus or saturate the intervention budget. Future work should stress-test the framework under orders-of-magnitude larger populations and adversaries who actively spoof causal edges.

Synthetic workload: The resource-sharing game abstracts energy dispatch and cloud bandwidth, but real grids include AC power-flow constraints, non-convex unit-commitment costs, and legal market rules. Porting AAF to such domains may require domain-specific norm predicates and rate-limited interventions to satisfy physical safety margins.

Compute footprint: Although the prototype meets a 5% CPU budget on EPYC and Cortex-A55 cores, embedded PLCs in industrial control may offer only tens of MHz of head-room. A tiny-ML re-implementation or a hardware cryptographic accelerator could mitigate this concern.

8.3 Ethical, Legal, and Social Implications

Privacy and surveillance. Recording every agent action invites *secondary use* risks. AAF mitigates the danger via keyed-hash digests, AES-SIV pseudonyms, and an escrowed identity table (§6). Nonetheless, deployers should carry out a data-protection impact assessment under GDPR Art. 35 and delete raw ring buffers once digests are anchored.

Over-deterrence and chilling effects. Reward penalties can skew agents toward risk-averse behavior, potentially lowering innovation in financial-market MAS [15]. A human-in-the-loop override—triggered by the yellow-flag dashboard—helps balance safety with exploration.

Procedural fairness. By design, Shapley-style attribution apportions blame according to marginal causal contribution. If agents differ in observability or computing power, this may correlate with protected attributes, leading to distributive inequity [38]. Auditors should therefore scrutinize $\rho_i(e)$ distributions for disparate impact.

8.4 Relevance to Emerging AI Governance

The EU AI Act (2024) and the NIST AI Risk-Management Framework (2023) both highlight collective emergent risks—but offer few technical recipes for tracing responsibility in networked AI systems. AAF operationalizes these policy aspirations by (i) anchoring an immutable event ledger; (ii) providing real-time statistical tests with formal α -level guarantees [27]; and (iii) linking those tests to proportionate, auditable interventions. Hence the framework can serve as a reference architecture for regulators drafting sector-specific codes of practice.

8.5 Future Directions

Scalable cryptography: Replacing Merkle DAG anchoring with succinct zero-knowledge roll-ups (e.g., Halo 2) could compress the storage footprint by an order of magnitude while enabling selective disclosure proofs.

Meta-norm adaptation: Current norms are fixed at deployment. An interesting extension is a meta-controller that tunes α , λ , and even the set Φ via constrained Bayesian optimization, subject to fairness and throughput SLAs.

Human-aligned explanations: While the Grafana DAG explorer provides low-level proofs, policy operators may prefer natural-language rationales. Coupling the ledger to an LLM-based explainer guarded by the event digests to prevent hallucination could bridge the accountability-interpretability gap [31].

Cross-domain generalization: Finally, deploying AAF in safety-critical cyber-physical systems, autonomous driving rings, or drone swarms where communication is intermittent and hard real-time deadlines exist would test the limits of the bounded-compromise theorem under severe timing jitter.

AAF demonstrates that cryptographically verifiable, statistically rigorous, and computationally light accountability is attainable in contemporary MAS. Yet translating the prototype into industrial and societal infrastructure requires careful attention to privacy guarantees, domain constraints, and human governance processes. These themes set the stage for interdisciplinary collaborations that we outline in the conclusion.

9 Conclusion and Future Work

This paper introduced an *Adaptive Accountability Framework* (AAF) that transforms a networked multi-agent system (MAS) into a *self-auditing socio-technical organism*. By uniting a tamper-evident Merkle ledger, Shapley-style responsibility scores, time-uniform sequential tests, and cost-bounded interventions, AAF provides—both in theory (Section 5) and practice (Section 7)—formal assurances that harmful emergent norms can be detected within a handful of control steps and suppressed below any designer-chosen ceiling η^* .

Key take-aways:

1. Causal tracing at scale: Cryptographically hashed event digests and constant-time Granger updates enable real-time provenance without saturating bandwidth: a 100-agent deployment needs only $\approx 80 \text{ KB s}^{-1}$.
2. Statistical robustness: An adaptive CUSUM calibrated by Robbins–Monro maintains a system-wide false-alarm rate of exactly α , even under 20% packet loss and non-stationary policies—extending classical Page–Lorden theory to decentralized MAS.
3. Cost-effective mitigation: Local reward shaping proportional to responsibility scores is sufficient to bound compromise and welfare loss, confirming the bounded-compromise theorem and eliminating the need for heavy global resets or retraining.
4. Practical viability: A production-grade reference stack, i.e., Python 3.11 + Rust/WASM + FoundationDB + Kafka, runs inside a 5% CPU budget on both EPYC and ARM Cortex-A55 hardware, paving the way for real deployments.

Limitations. Experiments focused on $N \leq 100$ agents in a stylized resource-sharing domain. Larger swarms, adversaries that spoof ledger messages, or safety-critical cyber-physical loops with sub-10 ms deadlines may breach current design margins. Moreover, the privacy model—keyed BLAKE3 hashes plus AES-SIV pseudonyms—assumes regulators can access the escrowed identity table; sectors with stronger secrecy requirements (healthcare, defense) will need stronger privacy-preserving ledgers (e.g. verifiable encrypted logs).

Road map for future work:

1. Learning-aware detectors: Integrate representation-learning or graph neural networks to flag coordinated drift that eludes low-dimensional statistics.
2. Zero-knowledge provenance: Replace Merkle anchoring with succinct zero-knowledge roll-ups (Halo 2, PlonK) so third-party auditors can verify norm violations without accessing raw hashes.
3. Human-aligned explanations: Couple the ledger to LLM-based explainers bounded by cryptographic proofs, producing natural-language rationales that satisfy emerging “AI-act notice” clauses.
4. Sector pilots: Field trials in power-grid balancing, hospital bed exchange, or high-frequency trading could surface domain-specific constraints (e.g., HIPAA data retention, MiFID II latency caps) and inform regulator guidance.
5. Ultra-large MAS: For $N \geq 10^4$ agents, delta-encoding, probabilistic sketches, and edge-aggregated detection will be needed; preliminary work suggests a 100-fold compression with Count-Min sketches and HyperLogLog without losing detection power.

Recent policy instruments—from the EU AI Act to NIST’s AI RMF—stress continuous, distributed oversight. AAF offers a concrete, open-source blueprint for that ambition: mathematically principled, cryptographically verifiable, computationally lean, and already validated on non-trivial MAS workloads. We hope the framework catalyzes interdisciplinary collaboration among control theorists, cryptographers, economists, and policy-makers as autonomous agents scale from dozens to millions in the infrastructures of tomorrow.

Appendix A. Detailed Proofs

This appendix provides full technical proofs for the results stated in Section 5. We restate the operational assumptions for ease of reference.

A1 Packet loss and delay: Each event tuple is dropped independently with probability $\varepsilon_{\text{loss}} \leq 0.2$ and, if delivered, is delayed by at most $\varepsilon_{\text{delay}} \in \{0, 1, 2, 3\}$ control steps.

A2 Bounded degree: The time-varying communication graph satisfies

$$\max_t \deg(G_t) \leq d_{\max} < \infty,$$

independent of the population size N .

A3 Diminishing learning rate: For every agent i the total-variation drift of its policy obeys $\|\pi_{i,t+1} - \pi_{i,t}\|_1 \leq \kappa t^{-\xi}$ with exponent $\xi > \frac{1}{2}$.

A4 Budgeted adversary: Adversarial agents harvest at most g_{\max} expected utility per step, whereas the supervisor may spend up to $c_{\max} > g_{\max}$.

Unless noted otherwise, all expectations and probabilities are taken with respect to the joint probability space that realizes environment dynamics, stochastic policies, packet loss, and observation noise.

A.1 Proof of Lemma 1

Statement recap: For any event e recorded in the ledger, $\sum_{i=1}^N \rho_i(e) = 1$ almost surely.

Proof 9 (Detailed proof.) Write $\mathcal{P}(e)$ for the set of all directed source-to- e paths in the causal-edge DAG and let $\mathcal{P}_i(e) \subseteq \mathcal{P}(e)$ denote those whose first edge originates from an action of agent i . Because the DAG has no directed cycles, every path in $\mathcal{P}(e)$ has precisely one distinct originating agent; thus the sets $(\mathcal{P}_i(e))_{i=1}^N$ form a disjoint partition of $\mathcal{P}(e)$. Then

$$\sum_{i=1}^N \rho_i(e) = \sum_{i=1}^N \frac{\sum_{p \in \mathcal{P}_i(e)} \beta^{|p|}}{\sum_{q \in \mathcal{P}(e)} \beta^{|q|}} = \frac{\sum_i \sum_{p \in \mathcal{P}_i(e)} \beta^{|p|}}{\sum_{q \in \mathcal{P}(e)} \beta^{|q|}} = 1,$$

where the final equality follows because the disjoint union of the $\mathcal{P}_i(e)$ is $\mathcal{P}(e)$. \square

A.2 Proof of Theorem 2

Statement recap: Under A1–A3 and fixed $0 < \beta < 1$ the responsibility estimate $\rho_i(e_T)$ converges almost surely to a limit $\rho_i^\infty(e)$ whenever the index of e_T satisfies $T - t(e_T) = O(1)$.

Proof 10 (Detailed Proof.) *Step 1: Eventual observation of edges.* Fix an event e and a causal path $p = \langle e_{k_0}, \dots, e_{k_m} = e \rangle$ of length $m \leq \ell_{\max}$; in our implementation $\ell_{\max} = 256$ equals the ring-buffer length. Because every edge traversal triggers at most one Granger test, edge $(e_{k_{j-1}} \rightarrow e_{k_j})$ is attempted exactly once. Under A1 the probability that the edge's record is available when the test is performed is $1 - \varepsilon_{\text{loss}}$. Hence all m edges in p are detected with probability $(1 - \varepsilon_{\text{loss}})^m \geq (1 - \varepsilon_{\text{loss}})^{\ell_{\max}} > 0$. The Bernoulli trials for distinct attempts are independent, so the indicator that any given edge is never observed has geometric tail. Let $X_p = \mathbf{1}\{p \text{ never fully observed}\}$.

Step 2: Borel–Cantelli. Because $\deg(G_t) \leq d_{\max}$ (A2) and $m \leq \ell_{\max}$, the number of candidate paths affecting e is bounded above by $M = d_{\max}^{\ell_{\max}} < \infty$. We have $\mathbb{P}[X_p = 1] \leq \varepsilon_{\text{loss}}^m$ for each p , so

$$\sum_{p \in \mathcal{P}(e)} \mathbb{P}[X_p = 1] \leq M \varepsilon_{\text{loss}}^{\ell_{\max}} < \infty.$$

The first Borel–Cantelli lemma therefore implies $\mathbb{P}[X_p = 1 \text{ infinitely often}] = 0$, i.e. every causal path is eventually observed almost surely (a.s.).

Step 3: Convergence of numerator and denominator. For each agent i define $N_{i,T} = \sum_{p \in \mathcal{P}_i(e)} \beta^{|p|} \mathbf{1}\{p \text{ observed by } T\}$. By Step 2, $N_{i,T} \rightarrow N_{i,\infty}$ a.s. as $T \rightarrow \infty$. Similarly $D_T = \sum_j N_{j,T} \rightarrow D_\infty = \sum_j N_{j,\infty}$ a.s. and $D_\infty > 0$ because at least one source agent acted. Consequently $\rho_i(e_T) = N_{i,T}/D_T \rightarrow \rho_i^\infty(e) = N_{i,\infty}/D_\infty$ almost surely by the continuous-mapping theorem. \square

A.3 Proof of Theorem 3

Statement recap: With threshold $h_t = h_0 + \sqrt{2 \log t}$ ($h_0 > 0$), the probability that a spurious causal edge is ever inserted is at most $\alpha = e^{-h_0^2/2}$.

Proof 11 (Detailed proof.) Under H_0 the m -lag Granger residual-variance ratio has exact F distribution $F(m, n-m)/m$ with $n = m + 1$ degrees-of-freedom [35, 26]. Let $U_t = \mathbf{1}\{F_t > h_t\}$. Then, by the Chernoff bound for χ^2 tails, $\mathbb{P}[U_t = 1] \leq e^{-h_t^2/2} = e^{-h_0^2/2} t^{-1}$. Taking the union bound over $t \geq 1$ yields

$$\mathbb{P}[\exists t: U_t = 1] \leq \sum_{t=1}^{\infty} e^{-h_0^2/2} t^{-1} = e^{-h_0^2/2},$$

as desired. Setting $h_0 = \sqrt{2 \log(1/\alpha)}$ recovers any target $\alpha \in (0, 1)$. \square

A.4 Proof of Theorem 4

Statement recap: With gain sequence $\eta_t = t^{-0.6}$ the adaptive CUSUM maintains long-run false-alarm frequency α .

Proof 12 (Detailed Proof.) Define $f(h) = \mathbb{P}_{H_0}(S \geq h) - \alpha$. The process $\{h_t\}$ satisfies the Robbins-Monro recursion $h_{t+1} = h_t - \eta_t f(h_t) + \eta_t \epsilon_{t+1}$ with martingale difference $\epsilon_{t+1} = Z_{t+1} - \mathbb{P}_{H_0}(S \geq h_t)$. Because S_t has bounded increments, ϵ_{t+1} is square integrable with $\mathbb{E} \epsilon_{t+1} = 0$ and $\sup_t \mathbb{E} \epsilon_{t+1}^2 < \infty$. Assumption $\sum_t \eta_t^2 < \infty$ ensures the Kushner-Clark condition, so $h_t \rightarrow h^*$ a.s. where $f(h^*) = 0$ [33]. Ergodicity of the CUSUM statistic under H_0 implies $\frac{1}{T} \sum_{t=1}^T \mathbf{1}\{S_t \geq h^*\} \rightarrow \mathbb{P}_{H_0}(S \geq h^*) = \alpha$, and dominated convergence gives the required limit for h_t . \square

A.5 Proof of Theorem 5

Statement recap: If $\lambda H \geq g_{\max} + \varepsilon$ the long-run compromise ratio satisfies

$$\limsup_{T \rightarrow \infty} C_T/T \leq \eta^* = \frac{\alpha H}{\lambda H - g_{\max}}$$

almost surely.

Proof 13 (Proof.) Let $Y_t = \mathbf{1}\{\phi(s_t, \mathbf{a}_t) = \text{violate}\}$ and define the compensated process $\tilde{Y}_t = Y_t - \eta^*$. Consider the random times τ_n at which interventions start and write $\Delta_n = \sum_{t=\tau_n}^{\tau_n+H-1} \tilde{Y}_t$. During window n the adversary can at most recover $g_{\max} H$ utility, whereas the supervisor spends λH . The net drift is therefore

$$\mathbb{E}[\Delta_n \mid \mathcal{F}_{\tau_n}] \leq \alpha H - (\lambda H - g_{\max}) < 0.$$

Define $M_t = \sum_{k=1}^t (\tilde{Y}_k - \alpha)$. Between interventions M_t has zero drift, and in mitigation windows it has negative drift; hence M_t is a super-martingale. Applying Doob's optional stopping at T and dividing by T yields $\mathbb{E}[C_T/T] \leq \eta^*$. Azuma-Hoeffding on bounded increments tightens this to almost-sure convergence.

Let the adversary invest exactly g_{\max} utility per step and cease activity during interventions. Renewal-reward arguments then show the ratio approaches η^* from below as $\lambda H \downarrow g_{\max}$, proving the bound is tight up to $O(\varepsilon^{-1})$.

A.6 Discussion of Assumption Sharpness

- A2 (Bounded degree): The proofs rely only on summability of path counts. A slowly growing degree bound, e.g. $\deg(G_t) = O(\log N)$, merely multiplies the constants in Lemma 1 and Theorem 2 by $\log N$; the qualitative guarantees survive.
- A3 (Diminishing learning rate): The exponent $\xi > \frac{1}{2}$ guarantees $\sum_t \|\pi_{i,t+1} - \pi_{i,t}\| < \infty$, which is sufficient for the bounded-difference martingale arguments. Empirically, RL schedulers such as Adam with a t^{-1} decay meet this requirement.
- A4 (Budget dominance): If $g_{\max} \geq c_{\max}$ an adversary can match or exceed the supervisor's corrective power, allowing $C_T/T \rightarrow 1$ in the worst case; no bounded-cost policy can prevent systemic capture. Thus the assumption is information-theoretically tight.

The lemmas and theorems above rigorously ground the empirical claims in Section 7: the ledger converges despite 20% packet loss, the detector maintains a 5% false-alarm rate, and inexpensive interventions provably cap long-run harm.

A.7 Proof of Corollary 2(Lorden Bound for Adaptive CUSUM)

Statement recap. For a persistent drift $\Delta > 0$ starting at τ^* we must show

$$\sup_{\tau^*} \mathbb{E}_{\tau^*}[T_{\text{alarm}} - \tau^* \mid T_{\text{alarm}} > \tau^*] \leq \frac{h^*}{\Delta - \delta},$$

where $h^* = \lim_{t \rightarrow \infty} h_t$.

Proof 14 Conditional on $h_t \rightarrow h^*$ (Theorem 4) the adaptive rule behaves like a fixed-threshold CUSUM with threshold h^* . Page's original result [48] bounds the expected delay by $h^*/(\Delta - \delta)$ when the post-change mean is $\mu_0 + \delta + \Delta$. Taking the supremum over τ^* yields the worst-case delay, completing the proof. \square

A.8 Proof of Proposition 1 (Minimal Penalty Magnitude)

Statement recap. For fixed window H and target compromise ceiling η^* the minimal penalty magnitude satisfies

$$\lambda_{\min} = \frac{g_{\max} + \alpha H}{H\eta^*}.$$

Proof 15 The upper bound in Theorem 5 reads $\eta^* = \alpha H / (\lambda H - g_{\max})$. Solving for λ gives $\lambda = (g_{\max} + \alpha H) / (H\eta^*)$. Monotonicity in λ implies this value is minimal. \square

A.9 Proof of Proposition 2 (Resource Complexity)

Statement recap. Storage grows as $O(T(N + d_{\max}h))$ and bandwidth as $O(N + d_{\max}h)$ bytes per step.

Proof 16 Each control step generates N event records (40 B each) plus at most $d_{\max}h$ causal-edge insertions (32 B hashes). Hence per-step storage is $O(N + d_{\max}h)$, giving the stated total after T steps. Gossip traffic forwards each record exactly once along each outgoing edge, bounding bandwidth by the same term. Constants are absorbed into the big- O . \square

Appendix B. Hyper-parameter Grid and HPC Job Script

- Grid definition: JSON file `experiments/grid.json` enumerates all $\langle N, \text{penalty}, \text{obs}, \alpha, \text{seed} \rangle$ tuples.
- Slurm launcher: Bash script `run_slurm.sh` submits an array job with `$SLURM_ARRAY_TASK_ID` indexing the JSON grid.

Appendix C. Micro-benchmark of Critical Kernels

Kernel	EPYC 7742 (μs)	Cortex-A55 (μs)
BLAKE3 hash (40 B)	0.38	2.9
Incremental Granger (m=8)	4.10	27.4
Merkle insert (depth 16)	1.22	9.8
CUSUM update (3 norms)	0.07	0.27
Responsibility recompute	0.44	3.1

All numbers are medians over 10^5 iterations. Full benchmark code is in `benchmarks/kernel_bench.rs` and `benchmarks/kernel_bench.py`.

Appendix D. Mirror-Descent Alert Budget Allocator

We model the per-norm false-positive budget as a simplex $w_t \in \Delta^{|\Phi|}$ updated by entropic mirror descent:

$$w_{t+1} = \frac{w_t \exp(-\eta z_t)}{\|\cdot\|_1},$$

where z_t is the zero-one loss vector of fired alerts. Standard analysis [23] yields regret $R_T \leq 2\sqrt{T \log |\Phi|}$; substituting $|\Phi| = 5$ and $T = 10^6$ gives $R_T \approx 10^{-2}$, hence the global alert budget $\bar{\alpha} = 0.05$ is never exceeded by more than 0.01 in our runs.

Appendix E. Derivation of Bandwidth and Storage Constants

Using the 40-byte record and 32-byte hash constants, the leading constant in Proposition 2 equals $40N + 32d_{\max}h$ bytes per step. With $N = 100$, $d_{\max} = 8$, $h = 8$ this evaluates to $40 \cdot 100 + 32 \cdot 8 \cdot 8 = 79 \text{ KB step}^{-1}$, matching the empirical figure reported in §7.

References

- [1] Mehdi Ahrarinouri, Mohammad Rastegar, and Ali Reza Seifi. Multiagent reinforcement learning for energy management in residential buildings. *IEEE Transactions on Industrial Informatics*, 17(1):659–666, 2021. doi: 10.1109/TII.2020.2977104.
- [2] Saad Alqithami. Adaptive accountability in networked multi-agent systems. In *Proceedings of the AAAI/ACM Conference on AI, Ethics, and Society*, volume 8, pages 127–137, Oct. 2025. doi: 10.1609/aaies.v8i1.36536. URL <https://ojs.aaai.org/index.php/AIES/article/view/36536>.
- [3] Giulia Andrijetho, Cristiano Castelfranchi, Eunate Mayor, John McBreen, Maite López-Sánchez, and Simon Parsons. (social) norm dynamics. In Giulia Andrijetho, Guido Governatori, Pablo Noriega, and Leendert W. N. van der Torre, editors, *Normative Multi-Agent Systems*, volume 4 of *Dagstuhl Follow-Ups*, pages 135–170. Schloss Dagstuhl–Leibniz-Zentrum für Informatik, 2013. ISBN 978-3-939897-51-4. doi: 10.4230/DFU.Vol4.12111.135.
- [4] Giulia Andrijetho, Guido Governatori, Pablo Noriega, and Leendert W. N. van der Torre, editors. *Normative Multi-Agent Systems*, volume 4 of *Dagstuhl Follow-Ups*. Schloss Dagstuhl – Leibniz-Zentrum f"ur Informatik, 2013. doi: 10.4230/DFU.Vol4.12111.
- [5] Matthew Arnold, Rachel K. E. Bellamy, Michael Hind, Stephanie Houde, Sameep Mehta, Aleksandra Mojsilovic, Ravi Nair, David Piorkowski, Darrell Reimer, and Alexandra Olteanu. FactSheets: Increasing trust in AI services through supplier's declarations of conformity. *IBM Journal of Research and Development*, 63(4/5):6:1–6:13, 2019. doi: 10.1147/JRD.2019.2942288.
- [6] Mark Bedau. Downward causation and the autonomy of weak emergence. *Principia: an international journal of epistemology*, 6(1):5–50, 2002. doi: 10.5007/1808-1711.2002v6n1p5.
- [7] Joppe W. Bos, Leo Ducas, Eike Kiltz, Vadim Lyubashevsky, John M. Schanck, Peter Schwabe, and Damien Stehlé. CRYSTALS–Kyber: A cca-secure module-lattice-based kem. In *Proceedings of the 2018 IEEE European Symposium on Security and Privacy (EuroS&P)*, pages 353–367, 2018. doi: 10.1109/EuroSP.2018.00032.
- [8] Manuele Brambilla, Eliseo Ferrante, Mauro Birattari, and Marco Dorigo. Swarm robotics: A review from the swarm engineering perspective. *Swarm Intelligence*, 7(1):1–41, 2013. doi: 10.1007/s11721-012-0075-2.
- [9] Lucian Buşoniu, Robert Babuška, and Bart De Schutter. A comprehensive survey of multiagent reinforcement learning. *IEEE Transactions on Systems, Man, and Cybernetics, Part C: Applications and Reviews*, 38(2):156–172, 2008. doi: 10.1109/TSMCC.2007.913919.
- [10] Jiajun Chai, Yuqian Fu, Dongbin Zhao, and Yuanheng Zhu. Aligning credit for multi-agent cooperation via model-based counterfactual imagination. In *Proceedings of the 23rd International Conference on Autonomous Agents and Multiagent Systems (AAMAS 2024)*, pages 281–289. International Foundation for Autonomous Agents and Multiagent Systems, 2024. doi: 10.5555/3635637.3662876.
- [11] Alan Chan, Carson Ezell, Max Kaufmann, Kevin Wei, Lewis Hammond, Herbie Bradley, Emma Bluemke, Nitarshan Rajkumar, David Krueger, Noam Kolt, Lennart Heim, and Markus Anderljung. Visibility into ai agents. In *Proceedings of the 2024 ACM Conference on Fairness, Accountability, and Transparency (FAccT 2024)*, pages 958–973. ACM, 2024. doi: 10.1145/3630106.3658948.
- [12] Ching-Chun Chang and Ichiro Echizen. The chronicles of foundation ai for forensics of multi-agent provenance. *arXiv preprint arXiv:2504.12612*, 2025. doi: 10.48550/arXiv.2504.12612.
- [13] Daniel D. Corkill. Collaborating software: Blackboard and multi-agent systems and the future. In *Proceedings of the International Lisp Conference*, pages 4070–4076, 2003.
- [14] Ali Dorri, Salil S. Kanhere, and Raja Jurdak. Multi-agent systems: A survey. *IEEE Access*, 6:28573–28593, 2018. doi: 10.1109/ACCESS.2018.2831228.
- [15] Florian Ederer and Gustavo Manso. Is pay for performance detrimental to innovation? *Management Science*, 59(7):1496–1513, 2013. doi: 10.1287/mnsc.1120.1683.
- [16] European Parliament and the Council of the European Union. Regulation (eu) 2024/1689 of 13 june 2024 laying down harmonised rules on artificial intelligence (artificial intelligence act), 2024. URL <https://eur-lex.europa.eu/eli/reg/2024/1689/oj/eng>. OJ L, 2024/1689, 12.7.2024.
- [17] Ferdinando Fioretto, Enrico Pontelli, and William Yeoh. Distributed constraint optimization problems and applications: A survey. *Journal of Artificial Intelligence Research*, 61:623–698, 2018. doi: 10.1613/jair.5565.
- [18] Jakob N. Foerster, Gregory Farquhar, Triantafyllos Afouras, Nantas Nardelli, and Shimon Whiteson. Counterfactual multi-agent policy gradients. In *Proceedings of the 32nd AAAI Conference on Artificial Intelligence (AAAI-18)*, pages 2974–2982. AAAI Press, 2018. doi: 10.1609/aaai.v32i1.11794.

[19] Cheuk Chi Kitty Fung, Qizhen Zhang, Chris Lu, Jia Wan, Timon Willi, and Jakob Foerster. Analysing the sample complexity of opponent shaping. In *Proceedings of the 23rd International Conference on Autonomous Agents and Multiagent Systems (AAMAS 2024)*, pages 623–631. International Foundation for Autonomous Agents and Multiagent Systems, 2024. doi: 10.5555/3635637.3662914.

[20] David K. Gifford. Weighted voting for replicated data. In *Proceedings of the 7th ACM Symposium on Operating Systems Principles (SOSP)*, pages 150–162, 1979. doi: 10.1145/800215.806583.

[21] Corrado Gini. *Variabilità e Mutabilità*. Tipografia di P. Cappini, Bologna, Italy, 1912.

[22] Balint Gyevnar, Cheng Wang, Christopher G. Lucas, Shay B. Cohen, and Stefano V. Albrecht. Causal explanations for sequential decision-making in multi-agent systems. In *Proceedings of the 23rd International Conference on Autonomous Agents and Multiagent Systems (AAMAS 2024)*, pages 771–779. International Foundation for Autonomous Agents and Multiagent Systems, 2024. doi: 10.5555/3635637.3662930.

[23] Elad Hazan. Introduction to online convex optimization. *Foundations and Trends® in Optimization*, 2(3-4):157–325, 2016. ISSN 2167-3888. doi: 10.1561/2400000013. URL <http://dx.doi.org/10.1561/2400000013>.

[24] Pablo Hernandez-Leal, Bilal Kartal, and Matthew E Taylor. A survey and critique of multiagent deep reinforcement learning. *Autonomous Agents and Multi-Agent Systems*, 33(6):750–797, 2019. doi: 10.1007/s10458-019-09421-1.

[25] Christopher D. Hollander and Annie S. Wu. The current state of normative agent-based systems. *Journal of Artificial Societies and Social Simulation*, 14(2):6 (pp. 1–6), 2011. doi: 10.18564/jasss.1750.

[26] Steven R Howard, Aaditya Ramdas, Jon McAuliffe, and Jasjeet Sekhon. Time-uniform chernoff bounds via nonnegative supermartingales. *Probability Surveys*, 17:257–317, 2020. doi: 10.1214/18-PS321.

[27] Steven R. Howard, Aaditya Ramdas, Jon McAuliffe, and Jasjeet Sekhon. Time-uniform chernoff bounds via nonnegative supermartingales. *Probability Surveys*, 17:257–317, 2020. doi: 10.1214/18-PS321. URL <https://doi.org/10.1214/20-PS344>.

[28] Anna Jobin, Marcello Ienca, and Effy Vayena. The global landscape of AI ethics guidelines. *Nature Machine Intelligence*, 1(9):389–399, 2019. doi: 10.1038/s42256-019-0088-2.

[29] Don Johnson, Alfred Menezes, and Scott Vanstone. The elliptic curve digital signature algorithm (ecdsa). Technical report, Certicom Research, 2001. URL <https://www.certicom.com/content/certicom/en/ecc-crypto/ecdsa.html>.

[30] Jules Kazil, David Masad, and Andrew Crooks. Mesa: An agent-based modeling framework. GitHub repository, <https://github.com/projectmesa/mesa>, 2019.

[31] Joshua A. Kroll, Joanna Huey, Solon Barocas, Edward W. Felten, Joel R. Reidenberg, David G. Robinson, and Harlan Yu. Accountable algorithms. *University of Pennsylvania Law Review*, 165(3):633–705, 2017. ISSN 0041-9907. doi: 10.2307/26600576.

[32] Sandeep S Kulkarni, Murat Demirbas, Deepak Madappa, Bharadwaj Avva, and Marcelo Leone. Logical physical clocks. In *Principles of Distributed Systems: 18th International Conference, OPODIS 2014, Cortina d’Ampezzo, Italy, December 16–19, 2014. Proceedings 18*, pages 17–32. Springer, 2014. doi: 10.1007/978-3-319-14472-6_2.

[33] H. Kushner and G.G. Yin. *Stochastic Approximation and Recursive Algorithms and Applications*. Stochastic Modelling and Applied Probability. Springer New York, 2003. ISBN 9780387008943. doi: 10.1007/b97441. URL <https://books.google.com.sa/books?id=EC2w1SaPb7YC>.

[34] Gary Lorden. Procedures for reacting to a change in distribution. *The Annals of Mathematical Statistics*, 42(6):1897–1908, 1971. doi: 10.1214/aoms/1177693055.

[35] Helmut Lütkepohl. *New Introduction to Multiple Time Series Analysis*. Springer, Berlin, Heidelberg, 2005. ISBN 978-3-540-26239-8. doi: 10.1007/978-3-540-27752-1.

[36] Ralph C. Merkle. A certified digital signature. *Advances in Cryptology—CRYPTO ’89*, pages 218–238, 1989. doi: 10.1007/0-387-34805-0_21.

[37] Margaret Mitchell, Simone Wu, Andrew Zaldivar, Parker Barnes, Lucy Vasserman, Ben Hutchinson, Elena Spitzer, Inioluwa Deborah Raji, and Timnit Gebru. Model cards for model reporting. In *Proceedings of the Conference on Fairness, Accountability, and Transparency (FAT* 2019)*, pages 220–229, 2019. doi: 10.1145/3287560.3287596.

[38] Brent Mittelstadt. Principles alone cannot guarantee ethical AI. *Nature Machine Intelligence*, 1(11):501–507, 2019. doi: 10.1038/s42256-019-0114-4.

[39] Andreassa Morris-Martin, Marina De Vos, and Julian Padgett. Norm emergence in multiagent systems: A viewpoint paper. *Autonomous Agents and Multi-Agent Systems*, 33:706–749, 2019. doi: 10.1007/s10458-019-09422-0.

[40] Chunyan Mu and Nir Oren. Measuring responsibility in multi-agent systems. *arXiv preprint arXiv:2411.00887*, 2024. doi: 10.48550/arXiv.2411.00887. Under review.

[41] Arun Sukumaran Nair, Tareq Hossen, Mitch Campion, Daisy Flora Selvaraj, Neena Goveas, Naima Kaabouch, and Prakash Ranganathan. Multi-agent systems for resource allocation and scheduling in a smart grid. *Technology and Economics of Smart Grids and Sustainable Energy*, 3(15), 2018. doi: 10.1007/s40866-018-0052-y.

[42] National Institute of Standards and Technology. Artificial intelligence risk management framework (ai rmf 1.0). Technical Report NIST AI 100-1, National Institute of Standards and Technology (NIST), January 2023. URL <https://nvlpubs.nist.gov/nistpubs/ai/nist.ai.100-1.pdf>.

[43] Andrew Y. Ng, Daishi Harada, and Stuart Russell. Policy invariance under reward transformations: Theory and application to reward shaping. In *ICML*, pages 278–287, 1999. doi: 10.5555/645528.657613.

[44] Jack O'Connor, Jean-Philippe Aumasson, Samuel Neves, and Zooko Wilcox-O'Hearn. The blake3 cryptographic hash function, 2020. <https://github.com/BLAKE3-team/BLAKE3>.

[45] Michael Oesterle, Tim Grams, Christian Bartelt, and Heiner Stuckenschmidt. Raise the bar: Restriction of action spaces for improved social welfare and equity in traffic management. In *Proceedings of the 23rd International Conference on Autonomous Agents and Multiagent Systems (AAMAS 2024)*, pages 1492–1500. International Foundation for Autonomous Agents and Multiagent Systems, 2024. doi: 10.5555/3635637.3663009.

[46] Ninell Oldenburg and Tan Zhi-Xuan. Learning and sustaining shared normative systems via bayesian rule induction in markov games. In *Proceedings of the 23rd International Conference on Autonomous Agents and Multiagent Systems (AAMAS 2024)*, pages 1510–1518. International Foundation for Autonomous Agents and Multiagent Systems, 2024. doi: 10.5555/3635637.3663011.

[47] Elinor Ostrom. *Governing the Commons: The Evolution of Institutions for Collective Action*. Cambridge University Press, Cambridge, UK, 1990. ISBN 978-0-521-40599-7. doi: 10.1017/CBO9780511807763. URL <https://doi.org/10.1017/CBO9780511807763>.

[48] E. S. Page. Continuous inspection schemes. *Biometrika*, 41(1/2):100–115, 1954. doi: 10.1093/biomet/41.1-2.100. URL <https://doi.org/10.1093/biomet/41.1-2.100>.

[49] Simone Parisi, Montaser Mohammedalamen, Alireza Kazemipour, Matthew E. Taylor, and Michael Bowling. Monitored markov decision processes. In *Proceedings of the 23rd International Conference on Autonomous Agents and Multiagent Systems (AAMAS 2024)*, pages 771–779. International Foundation for Autonomous Agents and Multiagent Systems, 2024. doi: 10.5555/3635637.3663015.

[50] Torsten Paulussen, Armin Heinzl, and Christian Becker. Multi-agent based information systems for patient coordination in hospitals. In *Proceedings of the International Conference on Information Systems (ICIS 2013)*, 2013. URL <https://aisel.aisnet.org/icis2013/proceedings/HealthcareIS/2>.

[51] Jon Perez-Cerrolaza, Jaume Abella, Markus Borg, Carlo Donzella, Jesús Cerquides, Francisco J Cazorla, Cristofer Englund, Markus Tauber, George Nikolakopoulos, and Jose Luis Flores. Artificial intelligence for safety-critical systems in industrial and transportation domains: A survey. *ACM Computing Surveys*, 56(7):1–40, 2024. doi: 10.1145/3626314.

[52] Jeremy Pitt, Julia Schaumeier, and Alexander Artikis. Axiomatization of socio-economic principles for self-organizing institutions: Concepts, experiments and challenges. *ACM Transactions on Autonomous and Adaptive Systems (TAAS)*, 7(4):1–39, 2012. doi: 10.1145/2382570.2382575.

[53] K.J. Prabuchandran, Hemanth A.N. Kumar, and Shalabh Bhatnagar. Multi-agent reinforcement learning for traffic signal control. In *Proceedings of the 17th International IEEE Conference on Intelligent Transportation Systems (ITSC)*, pages 2529–2534, 2014. doi: 10.1109/ITSC.2014.6958095.

[54] Iyad Rahwan, Manuel Cebrian, Nick Obradovich, Josh Bongard, Jean-François Bonnefon, Cynthia Breazeal, Jacob W. Crandall, Nicholas A. Christakis, Iain D. Couzin, Matthew O. Jackson, Nicholas R. Jennings, Ece Kamar, Isabel M. Kloumann, Hugo Larochelle, David Lazer, Richard McElreath, Alan Mislove, David C. Parkes, Alex “Sandy” Pentland, Margaret E. Roberts, Azim Shariff, Joshua B. Tenenbaum, and Michael Wellman. Machine behaviour. *Nature*, 568(7753):477–486, 2019. doi: 10.1038/s41586-019-1138-y.

[55] Siyue Ren, Zhiyao Cui, Ruiqi Song, Zhen Wang, and Shuyue Hu. Emergence of social norms in generative agent societies: Principles and architecture. In Kate Larson, editor, *Proceedings of the Thirty-Third International Joint Conference on Artificial Intelligence (IJCAI-24)*, pages 7895–7903. International Joint Conferences on Artificial Intelligence Organization, 8 2024. doi: 10.24963/ijcai.2024/874. URL <https://doi.org/10.24963/ijcai.2024/874>. Human-Centred AI.

[56] Herbert Robbins and Sutton Monro. A stochastic approximation method. *The Annals of Mathematical Statistics*, 22(3):400–407, 1951. doi: 10.1214/aoms/1177729586. URL <https://doi.org/10.1214/aoms/1177729586>.

- [57] Sandip Sen and Stephanie Airiau. Emergence of norms through social learning. In *Proceedings of the 20th International Joint Conference on Artificial Intelligence (IJCAI 2007)*, pages 1507–1512, 2007. doi: 10.5555/1625275.1625519.
- [58] Marc Serramia, Natalia Criado, and Michael Luck. Multi-user norm consensus. In *Proceedings of the 23rd International Conference on Autonomous Agents and Multiagent Systems (AAMAS 2024)*, pages 1683–1691. International Foundation for Autonomous Agents and Multiagent Systems, 2024. doi: 10.5555/3635637.3663029.
- [59] Jack Sherman and Winifred J. Morrison. Adjustment of an inverse matrix corresponding to a change in one element of a given matrix. *The Annals of Mathematical Statistics*, 21(1):124–127, 1950. doi: 10.1214/aoms/1177729898. URL <https://doi.org/10.1214/aoms/1177729898>.
- [60] Yoav Shoham, Robert Powers, and Trond Grenager. If multi-agent learning is the answer, what is the question? *Artificial Intelligence*, 171:365–377, 2007. doi: 10.1016/j.artint.2006.02.006.
- [61] Peter Stone, Manuela Veloso, and Michael Bowling. Multiagent systems: A survey from a machine learning perspective. In *European Conference on Machine Learning (ECML 2000)*, pages 140–150, 2000. doi: 10.1023/A:1008942012299.
- [62] Leigh Tesfatsion and Kenneth L. Judd. Agent-based computational economics: A constructive approach to economic theory. In Leigh Tesfatsion and Kenneth L. Judd, editors, *Handbook of Computational Economics, Volume 2: Agent-Based Computational Economics*, pages 831–880. North-Holland, 2006. doi: 10.1016/S1574-0021(05)02016-2.
- [63] Stelios Triantafyllou, Alekса Šuković, Debmalya Mandal, and Goran Radanovic. Agent-specific effects: A causal effect propagation analysis in multi-agent mdps. In *Proceedings of the 41st International Conference on Machine Learning (ICML 2024)*, pages 21831–21853. PMLR, 2024.
- [64] Sz-Ting Tzeng, Nirav Ajmeri, and Munindar P. Singh. Norm enforcement with a soft touch: Faster emergence, happier agents. In *Proceedings of the 23rd International Conference on Autonomous Agents and Multiagent Systems (AAMAS 2024)*, pages 1837–1846. International Foundation for Autonomous Agents and Multiagent Systems, 2024. doi: 10.5555/3635637.3663046.
- [65] Duncan J. Watts and Steven H. Strogatz. Collective dynamics of 'small-world' networks. *Nature*, 393(6684):440–442, 1998. doi: 10.1038/30918.
- [66] Jessica Woodgate, Paul Marshall, and Nirav Ajmeri. Operationalising rawlsian ethics for fairness in norm-learning agents. In *Proceedings of the 39th AAAI Conference on Artificial Intelligence (AAAI 2025)*, pages 26382–26390. AAAI Press, 2025. doi: 10.1609/aaai.v39i25.34837.
- [67] Michael Wooldridge. *An Introduction to MultiAgent Systems*. John Wiley & Sons, 2nd edition, 2009.
- [68] Michael Wooldridge and Nicholas R. Jennings. Intelligent agents: Theory and practice. *The Knowledge Engineering Review*, 10(2):115–152, 1995. doi: 10.1017/S0269888900008122.